International Journal of Scientific Research in Science, Engineering and Technology (www.ijsrset.com)
© 2020 IJSRSET | Volume 7 | Issue 2 | Print ISSN: 2395-1990 | Online ISSN : 2394-4099
DOI : https://doi.org/10.32628/IJSRSET19648

Software-Engineering Optimization with Mathematical Method Improvements for Numerical Reuleaux Method

Francisco Casesnoves PhD Engineering MSc Physics MD*[1]

*[1] Independent Bioengineering-Medical-Software and Medical Devices Researcher, COE, Tallinn University of Technology, Tallinn, Harjumaa, Estonia

ABSTRACT

This paper presents an extension both in software optimization with simulations and detailed mathematical theory of Numerical Reuleaux Method based on previous publications. In the literature, there are a number of papers in Numerical Reuleaux Method and its applications (Aerospace, Helicopter Dynamics in Turbulence Conditions, Biomedical Engineering, Biomechanics, etc) since 2007. This contribution is a detailed presentation of the mathematical framework that constituted the basis for those articles along 2007-2020. The Classical Reuleaux Method (**CRM**) is frequently used in Physical Dynamics, Engineering Mechanics and Bioengineering to determine the Instantaneous Rotation Center (**IRC**) of a rigid body in arbitrary movement. The generic mathematical **CRM** only can be applied on rigid bodies, whose shape remains constant during the movement. If the solid in movement is a Pseudo-Rigid Body (**PRB**), the **CRM** has to be modified numerically to conform the shape changes and adapt on the density distribution variations of the **PRB** (we denominate it, in this case[1], **The Numerical Reuleaux Method**, **NRM**). This Geometrical-Numerical Approximation Method is based on the division of the Pseudo-rigid body into small volume parts called voxels (roughly speaking parallelepipedic), namely, voxelization of the body subject to dynamics. The theoretical basis of the method is strictly shown in complementary details, with the necessary Theorems and Propositions of the model. Nonlinear Optimization Techniques that support the initial theory have been developed, and the Error boundaries with Error reduction techniques are determined. Computational Simulations have been carried out to prove the **NRM** Theoretical Model feasibility and numerical veracity of the Propositions, Theorems, and Error Boundaries. Appropriate software was made to carry out these simulations conveniently. The initial results agree to the theoretical calculations, and the IRC computation for 2 voxels shows to be simple and easy. Some initial guidelines for a theoretical development of this algorithm applied on large pseudo-rigid bodies, by using Monte-Carlo techniques, are sketched. Recent applications, Aerospace and Biomechanics, are also shown.

Keywords : IRC, Nonlinear Optimization, Numerical Reuleaux Method (NRM), Voxel, Pseudo-rigid Body, Numerical Simulations.

I. INTRODUCTION

The Classical Reuleaux Method is used for the determination of the IRC of rigid bodies [**38**,**39**]. This method is basically geometrical [**Fig 1**], and the IRC is given by the unique intersection point of two lines (for **2D**), or three planes (for **3D**). These lines (or planes in **3D**), are perpendicular at the middle points

of the straight segments that join some points, (two segments and four points that define these segments in **2D**, and three segments, with six points that define the segments in **3D**), of the initial position of the body, with the corresponding ones which are at the final position of the body.[NOTE, large Figures are set in Appendix Section with Computational Tables].

However, when the body in movement is a **PRB**, the method needs to be modified into a numerical way. This implies that the shape of the pseudo-rigid body has to be divided into small volume parts called voxels, and the initial algorithm [**21**,**32**,**33**,**45**] is applied for calculating the particular IRC for each independent voxel[2] [**Fig 3**]. The optimal IRC for the complete **PRB** is given by that point whose sum of distances to all those individual IRCs (that is, the IRC for each voxel movement), is minimal [**24**]. It is also obliged to take into account the changes in the mass and density distribution into the pseudo-rigid body. This matter makes the calculations more complicated, although some approximations can be applied. Previous publications of this **NRM**, with a radiological experimental verification series of experiments, have been focused on Bioengineering applications related to Biomechanical properties of the human spine [**11**].

We developed two Objective Functions. Both Objective Functions are set as a Least-Squares Algorithm, but with different weight factors. The Second Objective Function explicit Formula is the same in its L_2 Norm term, but the weight factor is purely related only to volume variation of the pseudo-rigid body.

The simulations carried out for 1 and 2 voxels frames show a clear difference of Error decrease in favour of the 2 voxels choice. The average difference of error both for **2D** and **3D** is about **8%**. Finally, some mechanical Engineering and Bioengineering (Biomechanics in particular, [**11**]) applications are show in brief. All in all, we consider this **NRM** model as a promising one for future industrial applications.

of the IRC of rigid bodies [**38**,**39**]. This method is basically geometrical [**Fig 1**], and the IRC is given by the unique intersection point of two lines (for **2D**), or three planes (for **3D**). These lines (or planes in **3D**), are perpendicular at the middle points of the straight segments that join some points, (two segments and four points that define these segments in **2D**, and three segments, with six points that define the segments in **3D**), of the initial position of the body, with the corresponding ones which are at the final position of the body.

However, when the body in movement is a **PRB**, the method needs to be modified into a numerical way. This implies that the shape of the pseudo-rigid body has to be divided into small volume parts called voxels, and the initial algorithm [**21**,**32**,**33**,**45**] is applied for calculating the particular IRC for each independent voxel[2] [**Fig 3**]. The optimal IRC for the complete **PRB** is given by that point whose sum of distances to all those individual IRCs (that is, the IRC for each voxel movement), is minimal [**24**]. It is also obliged to take into account the changes in the mass and density distribution into the pseudo-rigid body. This matter makes the calculations more complicated, although some approximations can be applied. Previous publications of this **NRM**, with a radiological experimental verification series of experiments, have been focused on Bioengineering applications related to Biomechanical properties of the human spine [**11**].

We developed two Objective Functions. Both Objective Functions are set as a Least-Squares Algorithm, but with different weight factors. The Second Objective Function explicit Formula is the same in its L_2 Norm term, but the weight factor is purely related only to volume variation of the pseudo-rigid body. The simulations carried out for 1 and 2 voxels frames show a clear difference of Error decrease in favour of the 2 voxels choice. The average difference of error both for **2D** and **3D** is about **8%**. Finally, some mechanical Engineering and Bioengineering (Biomechanics in particular, [**11**])

applications are show in brief. All in all, we consider this **NRM** model as a promising one for future industrial applications.

In summary, this paper presents all the mathematical and computational background of Numerical Reuleaux Method that was made in its first year of foundations (2007). It is complemented with Aerospace and Biomedical applications and details. Therefore, any article of this subject that can be found in the international scientific literature, can be better understood with all these algorithms and software-engineering numerical data and simulations (Tables 1-5, and Figure 10 at Appendix).

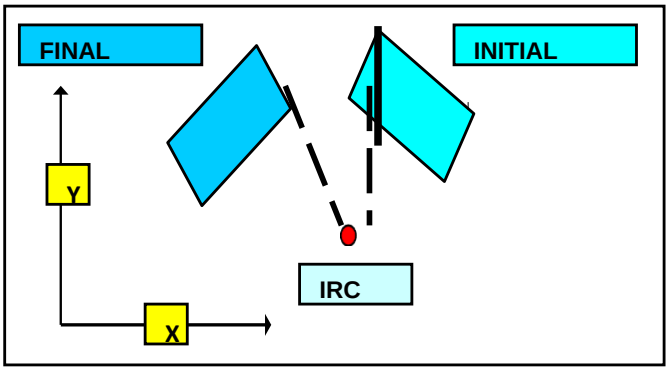

Fig 1.-Basic sketch of the **CRM** [**10**] in **2D** for a rigid body. The Reuleaux segments join two points of the body at the initial position, with the corresponding ones at the final position. The perpendiculars to these segments at their middle points intersect at the exact **IRC**. In **2D** the **IRC** is given by the intersection of two perpendiculars, and we have to take at least two points of the rigid body. In **3D** the **IRC** is given, instead, by the intersection of three planes (Bisecting Planes), which are perpendicular to the Reuleaux segments middle points (three) [**11**]. The necessary condition in **3D** is the **PRB** to perform a pure movement in **3D** (different variations of the three spatial Cartesian Coordinates), otherwise we would obtain a rotation axis or a simple translation, and in other cases the computing program running becomes complicated by the singularity of a matrix. This matrix is used to obtain the solution of a Linear System of Equations rather Ill-posed [**16**,**23**] if the meshing of the Reuleaux segments in **3D** is not selected properly.

[1] The name of Numerical Reuleaux Method (**NRM**) is assigned to recognize the solid foundation of the Classical Reuleaux Method (**CRM**), wisely invented by the Engineer **Franz Reuleaux** (1829-1905) [**38**,**39**]. In addition, it is obliged to cite other important contributions (among many of them), such as Schröder, J (1899) [**42**], Kennedy, A (1881) [**25**], Clark, WM, and Virginia Downward (1930) [**15.1**], and Rankine, W (1887) [**37**].

[2] The modification of the Classical Reuleaux Method for Rigid Bodies in **2D** to the **NRM** for Pseudo-Rigid Bodies, was invented and designed mathematically by F Casesnoves during February 2007, at Biomechanics Lab of Mechanical Engineering Department (Nottingham University, UK). The origin of the idea came from an initial Spinal Biomechanics problem. That is, the changes in volume that occur in artificial implants during the spine movements (mainly pure flexion and extension).

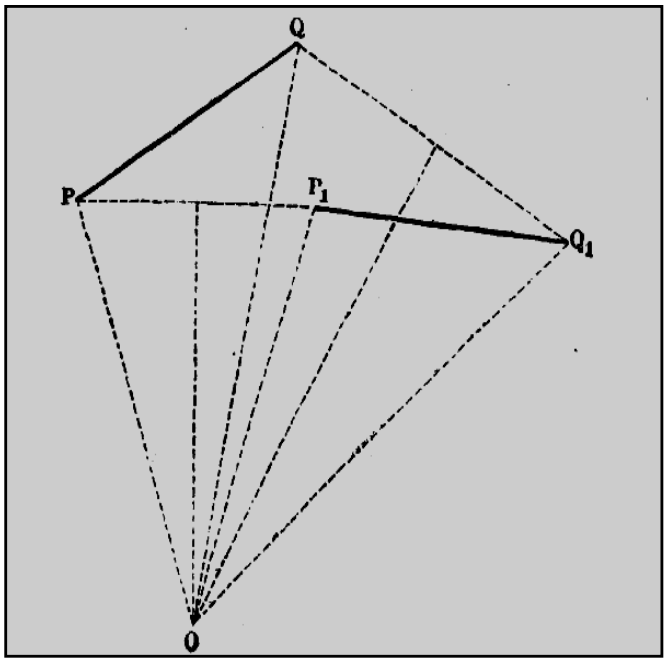

Fig 2.-Representation of the original historic geometrical definition of IRC in 3D by the Classical Reuleaux Method, as it was sketched in Kinematics of Machinery (McMillan & Co., London [38], English

version of previous German publications [38,39]). Reuleaux set the concept of Temporary Centre, which is equivalent to IRC, and defined the geometrical concept of Central Polygon by 1876. Note that the sketch corresponds to a wire PQ (a straight line in approximation, if we despise the caliber-related volume), in a 3D movement. In this approximation, it is only necessary to take two points of the wire, since a straight line is defined in the space by two points [46]. Usually, in 3D, we have to work with three points, because a solid-body position is defined in the space by at least three points [1.1].

1.1-Theoretical Introduction and Concepts

Therefore, the classical Reuleaux method cannot be applied on to resolve the IRC problem when the body in movement is Pseudo-rigid, because of the shape of the **PRB** is changing arbitrarily [**Fig 3**]. The necessary and compulsory modification is to divide the pseudo-rigid body into voxels, and compute independently their respective IRCs. The final step is to find with computational methods and proper software, that point whose sum of distances to all those IRCs is minimal if we use an Optimization Least-squares Method (**LSM**) [**19**,**43**, **27**]. Other types of Optimization, by using Statistical concepts, or different techniques, such as Minimax (or Tchebycheff Norms Methods, [**33**]), are feasible to be carried out. All in all, the selected **LSM** can be proven with mathematical theorems, based on geometric calculations and fundamental Optimization Theory. Previous Contributions are based on science history. Reuleaux started to publish his both Theoretical and Geometrical investigations by 1876 [**38**,**39**]. However, there are more contemporary researchers to Reuleaux and during the 20th Century who also have carried out significant contributions to the same investigation area. We can recall the works of Schröder, J (1899) [**42**], Kennedy, A (1881) [**25**], Clark, WM, and Virginia Downward (1930) [**15.1**], and Rankine, W (1887) [**37**]. Most of them analysed the work of Reuleaux and also developed further advances related to his Theories. It is a matter of fairness to recognize also their contributions, among several others. We present a series of **Fig 3 Complementary** to catch up better the concepts.

1.2.-Previous Contributions

Reuleaux started to publish his both Theoretical and Geometrical investigations by 1876 [**38**,**39**]. However, there are more contemporary researchers to Reuleaux and during the 20th Century who also have carried out significant contributions to the same investigation area. We can recall the works of Schröder, J (1899) [**42**], Kennedy, A (1881) [**25**], Clark, WM, and Virginia Downward (1930) [**15.1**], and Rankine, W (1887) [**37**]. Most of them analysed the work of Reuleaux and also developed further advances related to his Theories. It is a matter of fairness to recognize also their contributions, among several others. We present a series of **Fig 3 Complementary** to catch up better the concepts.

1.3.-Research Objectives

The principal aim of this paper is to develop a truly theoretical model to determine the **IRC** of any pseudo-rigid body in movement. The numerical basis and demonstrations for this **NRM** model are based on a rigorous mathematical development, and subsequently on accurate random simulations. Both stages are compulsory to carry out a logic proof, although the first mathematical demonstration constitutes the initial necessary condition. The model optimization can be made by several objective functions, and two types of them are presented in this contribution. The weight factors selections constitute an important part of these objective functions [**32**, **33**]. The second objective is to carry out a primary trial of Simulations for 1 and 2 voxels, both in **2D** and **3D**. Once the results obtained, we will compare the average error values differences between the frame corresponding to 1 voxel, and the 2 voxels one. It is very important to find and set a clear difference between the average errors [**21**,**29**,**45**], in favour of the higher number of voxels choice.

1.4.-Results Overview

The synthesis of the results can be classified into two parts. The first one is related to the mathematical development of the model, and the second to the accuracy of the simulations data. The mathematical model and the nonlinear optimization carried out can be considered rigorously acceptable because the formal conditions to demonstrate the **Convexity** of the objective function, and the smoothness of the Nonlinear Optimization have been proven. These other properties are, namely, **Gateaux Differentiability**, **Frechet Differentiability**, and **Strict Differentiability** [**5.2**]. The different Differentiability properties that have been proven are complemented with clear explanations about why and how these concepts imply the smoothness of the Optimization both theoretical and computational calculations.

The **Existence** and **Uniqueneness** of the solution if the movement is in **3D** (for a pure **2D**-movement the solution is a straight line, an axis of rotation) has been demonstrated. The final formula that gives the **Global Minimum** [**5.2**, **32**] has been determined. The inequalities developed to find out the Superior Error Boundaries have also been mathematically checked.
The results obtained through simulations agree initially to the model theory. The intuitive idea related to the numerical discretization concept (that is, the greater number of voxels, the lower error magnitudes), is corroborated by the numerical data obtained.

The practical Simulations results show a clear error reduction when the number of voxels increases, both in **2D** and **3D**. In **2D**, we find an Error reduction (≈**6%**) when the **PRB** is divided into 2 voxels [**45**,**29**]. The difference in **3D** is higher, and there is a clear Error reduction (≈**10%**) when the number of voxels increases. However, we consider these simulations stage as a primary attempt, because longer and improved Simulations Trials and Statistics will be necessary to set a contundent proof of the theory.

In particular, new software has been planned to fix a random initial position of the **PRB** in the **3D** space, followed by a random rotation and volume changes. On the whole, the theory of the model has been implemented with promising results for future industrial applications [**11**].

II. Mathematical Model

In this Subsection we present clearly the basic concepts and properties of the Mathematical Model. Two Objective Functions are defined with their corresponding weight factors. Finally, a simple Theorem that fixes the relationship and Geometrical convergence between the **CRM** and the **NRM** is demonstrated.

2.1.-General Settings. Initial Assumptions

Before to start with the demonstration of a number of Theorems, it is necessary to prove some initial premises, that constitute the base of the Numerical Reuleaux Method for a **PRB**. Then, we assert the following,

When a **rigid body** performs an arbitrary movement, the **CRM** IRC corresponding to that path, **is just the same** than those multiple IRCs, which can be obtained by the Reuleaux Method, applied on each voxel that constitutes the complete rigid body.

Proof.-It is simply geometrical and evident. Those two points that lie on the half of the segments, which join the initial and final movements of the rigid body, define the chord of a circle whose center is the IRC [**Fig 2**]. If we divide the rigid body into several voxels, and carry out the same geometrical calculations, all the corresponding IRCs are just the same and center-coincident [**Fig 4**]. Those circles have different radii, but the same center, that is, are concentric, because the Reuleaux- segments are parallel lines [**Fig 4**].

When a rectangular semi-rigid body performs an arbitrary movement, however, there are variation of density into its whole body, which cause an irregular

distribution of density in each voxel that constitute the total semi-rigid body. Therefore, when the **NRM** is applied on, it is not only necessary to consider the changes of shape, but also of density distribution.

2.2.-Objective Function(s) Definition

Once the concept has been set, we will show a simple idea of the First Objective Function and how it works physically and mathematically. The accuracy of this example has been reduced, and the main intention is to make a quick caption of the model settings.

The graphical definition of the Mathematical Model for the Numerical Reuleaux Method is displayed in [**Fig 1**]. Complementary, it is shown a basic formula for the calculation of the Numerical Reuleaux Method for the IRC in [**Equation 1**]. In [**Fig 5**], we show in a explicit form, the calculation for the optimal IRC corresponding to the scheme of [**Fig 1**], that is, it is drawn those two IRCs points of the [**Fig 1**], and the chosen coordinates system. In this extremely simple scheme, the Numerical Reuleaux Model (a least-squares model) reads

$$f(X)=\frac{m_1}{m_1+m_2}X^2+\frac{m_2}{m_1+m_2}(d-X)^2$$

[Equation 1]

where $m_1/(m_1+m_2)$ and $m_2/(m_1+m_2)$ are the weight factors (in the masses of the rectangular pseudo-rigid body after the movement) corresponding to the density variations distribution, and **d** is the distance between the two IRCs of each voxel. The coordinate **X** gives the distance from the IRC(1) to the IRC(2). The model presented is based on two main assumptions

There are changes in the shape of a pseudo-rigid body in any arbitrary movement

-There are variations in the density distribution of the pseudo-rigid body also when moving

We will define two Objective Functions. The First one is the Mass-related Objective Function, and the Second one is the denominated the Volume-related Objective Function. According to these premises, we start defining also the following differential distribution of densities

$$m_1=\int_{V_1}\rho_1(\vec{r})dv$$

[Eq 2]

and

$$\boldsymbol{m_2=\int_{V_2}\rho_2(\vec{r})dv}$$

[Eq 3]

where ρ_i **i=1,2** are the density distribution of each voxel, superior and inferior respectively. When the number of voxels increases to **i** voxels, the First Objective Function Mass-related, as a result, is formed by vectorial functions and has three dimensions [**17**,**18**,**46**,], namely

$$f(x)=\sum_{i=1}^{n}\frac{m_i}{\sum_{j=1}^{n}m_j}\times\left\|\vec{x}-\vec{x_i}\right\|$$

[Eq 4]

or

$$f(\vec{x})=\sum_{i=1}^{n}\frac{\int_{V_i}\rho_i(\vec{x_i})dv}{\sum_{j=1}^{n}\int_{V_j}\rho_j(\vec{x})dv_j}\times\left\|\vec{x}-\vec{x_i}\right\|^2$$

[Eq 5.1]

where ρ_i **i=1,2,..n** and ρ_j **j=1,2,….n** are the corresponding density functions for each voxel. This is the generalization of the mathematical model for **n** voxels. The weight factors are expressed in a differential distribution of densities in **[Eq 5.1]**.

Therefore, we have given the initial definitions for setting two Objective Functions. If the pseudo-rigid body is divided into voxels (**3D**), or pixels (**2D**), each one, **i**, of them will have a differential density distribution (ρ_i), whose volume-integration (**3D**) will give the complete mass of each voxel. The density distribution (**dd**) [**Eqs 2,3**] for the weight factors of the First Objective Function, is the difference between the final position voxel differential density function, and its corresponding initial voxel position

differential density function. That is, a difference-differential density function (**ddf**). The differential density **dd** for the initial position is defined only for the initial volume voxel (rest of the space is null), and the same occurs for the final position **dd**. According to these definitions, we have set the Objective Functions. Both Objective Functions are set as a Least-Squares Algorithm, but with different weight factors. The First Objective Function [**Eq 5.1**] is a explicit vectorial function (three variables), which is equal to a summatory from **i=1** to **N** (number of voxels, in **2D** would be the number of pixels, with a surface-integration). Each member of the summatory is related to a voxel, **i**, of the pseudo-rigid body, and is equal to the product of a Coefficient (weight factor) by the square of the L_2 Norm (Least-Squares Method), that expresses the difference between the optimal vector (to be determined by the optimization method), and the vector defined by the IRC position of that particular voxel (or pixel). The weight factor of the First Objective Function for each voxel **i**, is equal to the quotient between the volume-integral of the **ddf** for that voxel volume, and the summatory of all the volume- integrals, from **i** to **N**, for all the voxels of the pseudo-rigid body. The volume-integration limits are taken for the maximum volume value, which can correspond to the final position voxel (pseudo-rigid body expansion), or to the initial position voxel (pseudo-rigid body contraction). In this way, the smaller volume (either initial or final voxel) is into the bigger volume of integration, and the **ddf** has one of its parts null at the domain outside the smaller volume.

The Second Objective Function (Volume-related) explicit Formula reads

$$f(\vec{x}) = \sum_{i=1}^{n} \frac{|\Delta V|}{\sum_{j=1}^{n} |\Delta V_j|} \times \left\| \vec{x} - \vec{x}_i \right\|^2$$

[**Eq 5.2**]

were ΔV_j corresponds to any difference between the initial volume of the voxel, and the final volumen of the voxel. Values are taken in absolute magnitude.

This Second Objective Function explicit Formula [**Eq 5.2**], [**1.2**,**2**,**3**,**7**,**14**,**32**], is the same in its L_2 Norm term [**Eq 5.1**], but the weight factor is purely related only to volume variation of the **PRB**. This factor is a quotient whose numerator is the absolute value of the volume increment between the initial volume of the voxel (initial position of the pseudo-rigid body), and the final volume of the voxel (final position, after the movement, of the pseudo-rigid body). The weight factor denominator, as seen, is formed by the summatory of all the absolute values of volume increments for all voxels of the pseudo-rigid body, from **i=1** to **N**.

2.3.-Convergence from the NRM to CRM

Theorem 1.-If The Numerical Reuleaux IRC of a pseudo-rigid body is applied on, its IRC tends towards the Reuleaux IRC of a rigid body when some specific distances (h_i) and angles (θ_i) tend to zero, namely

$$h_i \to 0$$
$$and$$
$$\theta_i \to 0$$

where h_i is the variation of height of the voxel from the rigid body size to the pseudo-rigid body size, and θ_i is the angle between the Reuleaux segments of the rigid and pseudo rigid-body voxel.

Proof.-This proof is graphical, very simple and intuitive [**9**]. We see in [**Fig 3**] the basic scheme of this demonstration. It is sufficient to prove the Theorem for the superior voxel ABCD. If the body is rigid, the voxel goes to the position A'B'C'D'. However, if the body is pseudo-rigid, the voxel ABCD goes to B'C'D'. Let be AA' the Reuleaux segment for the rigid body, which form an angle θ with the AD' Reuleaux segment of the pseudo-rigid body. It is evident geometrically that **h**, the distance A'D' has the following properties

$$h \to 0 \ and \quad \theta \to 0$$

When the deformation of the body tends to decrease. That is, the Reuleaux segment for the pseudo-rigid body AD' tends to the Reuleaux segment AA' of the rigid body, and therefore the Theorem is proven.

In the following, the theoretical study of the Numerical Reuleaux model involves the analysis of the characteristics of the objective function. These are related to the convexity properties, the local and global minima existence, and the determination of the errors. There are two types of errors, the first related to the variation of density, and the second to the shape changes. All these theoretical results can be applied on the experimental results and simulations of the model, and also in the construction of the computational software for the final practical stages.

The analysis of the convexity in an objective function, previously to carry out the complete optimization method, constitutes a crucial point that determines part of the final results. When we demonstrate that a function is convex, it follows straightforward that it is possible to find at least local minima in the optimization calculations. If we also demonstrate that it is possible to find a global minimum among those local minima, the final results can be considered acceptable.

III. Objective Function(s) Mathematical Properties

This Section deals with the mathematical demonstration of the most important properties of the Objective Function to carry out a rigorous and feasible Optimization Method. Among them, the most important is the Convexity of the model. When a Nonlinear Objective Function is Convex, we can assert that a Global Minimum can be obtained through suitable optimization. In addition, we prove other properties, such as the **Gateaux Differentiability**, **Frechet Differentiability**, and **Strict Differentiability** [**5.2**]. The mathematical significance of these properties in an objective function is related to get useful information about how the minimum of the objective function can be computationally reached. That is, the smoothness, the speed, and the geometrical availability of arbitrary directions towards to catch up the Global Minimum. The order in which they have been cited goes from more relaxed conditions (**Gateaux Differentiability**) towards tougher mathematical conditions (**Strict Differentiability**).

$$-k_1(1-\lambda)^2x_2^2 - k_2(1-\lambda)^2x_2^2 + \dots$$
$$\dots + (1-\lambda)x_2^2 = \dots$$
$$\dots = x_2^2 \times (1-\lambda) \times [1-(1-\lambda)] = \dots$$
$$\dots = x_2^2(1-\lambda)\lambda$$

1) 1.-Model Convexity

We show the following **Proposition 1**, to demonstrate the Covexity of the Model. The proof is rather long, but not difficult.

Proposition 1.-The objective function of the Numerical Reuleaux model is a convex function, namely

$$f(\lambda \overrightarrow{x_1} + (1-\lambda)\overrightarrow{x_2}) \leq \lambda f(\overrightarrow{x_1}) + (1-\lambda) f(\overrightarrow{x_2})$$
$$for$$
$$\lambda \in (0,1)$$

[Eq 6]

Proof.-We will prove this with the most simple case of a one-dimensional function. The demonstration can also be extended on the **2D** and **3D** cases. We have, initially, to develop both parts [**32**] of the inequality

$$f(\lambda x_1 + (1-\lambda)x_2) \leq \lambda f(x_1) + \\ + (1-\lambda) f(x_2)$$

[Eq 7]

The left hand of this inequality in one dimension is

$$f(\lambda x_1 + (1 \quad \lambda)x_2) = k_1 \times (\lambda x_1 + \\ + (1 \quad \lambda)x_2)^2 [Part\ 1] + \\ + k_2 \times (d \quad (\lambda x_1 + (1 \quad \lambda)x_2))^2 [Part\ 2]$$

$$k_1 = \frac{m_1}{m_1 + m_2}$$

$$and$$

$$k_2 = \frac{m_2}{m_1+m_2}$$

[Eq 9]

Hence, the first part is equal to

$$k_1 \times (\lambda x_1 + (1-\lambda)x_2)^2 = k_1\lambda^2 x_1^2 + \\ +k_1(1-\lambda)^2 x_2^2 + 2\lambda(1-\lambda)x_1 x_2 k_1$$

[Eq 10]

And the second part

$$k_2 \times (d - (\lambda x_1 + (1-\lambda)x_2))^2 = \\ = k_2 \times d^2 + \lambda^2 k_2 x_1^2 + \\ +k_2(1-\lambda)^2 x_2^2 + \\ +2\lambda(1-\lambda)k_2 x_1 x_2 - \\ -2\lambda k_2 d x_1 - 2(1-\lambda)d k_2 x_2$$

[Eq 11]

Now, we are dealing the right hand of the unequality

$$\lambda f(x_1)[Part1] + (1-\lambda)f(x_2)[Part2]$$

[Eq 12]

So we have the first part

$$\lambda f(x_1) = \lambda[k_1 x_1^2 + k_2(d-x_1)^2] = \lambda k_1 x_1^2 + \\ \lambda k_2 d^2 + \lambda k_2 x_1^2 - 2\lambda k_2 d x_1$$

[Eq 13]

And the second part

$$(1-\lambda)f(x_2) = (1-\lambda)k_1 x_2^2 + (1-\lambda)k_2 d^2 + (1- \\ \lambda)k_2 x_2^2 - 2(1-\lambda)k_2 x_2 d$$

[Eq 14]

Now, we are going to share those terms that are equal in both sides of the unequality, and carry out further calculations to demonstrate that the convexity unequality holds for all the selected space. There is a group of terms that cancel each other, and the others have to be conveniently combined.

We have in the **[Eq 11]** the following term

$$k_2 d^2$$

[Eq 15]

And in **[Eq 13]** and **[Eq 14]**

$$\lambda k_2 d^2 \\ and \\ (1-\lambda)k_2 d^2$$

[Eq 16]

These two last terms sum is equal to the term of **[Eq 15]**, so they cancel each other. Now, the following group of terms:

In the **[Eq 11]**

$$-2\lambda k_2 d x_1 - 2(1-\lambda)d k_2 x_2$$

[Eq 17]

And in the **[Eq 13]** and **[Eq 14]**

$$-2\lambda k_2 d x_1$$

[Eq 18]

with

$$-2(1-\lambda)k_2 x_2 d$$

[Eq 19]

So we see that the terms of **[Eq 11]** cancel the terms of **[Eq 18]** and **[Eq 19]** respectively. Now the group of terms that have to be shared together to demonstrate the unequality. We have in **[Eq 10]** the term

$$k_1\lambda^2 x_1^2$$

[Eq 20]

And in the **[Eq 11]** just the same term

$$k_2\lambda^2 x_1^2 \\ but \\ k_1 + k_2 = 1$$

[Eq 21]

So, we can pass these terms to the right side of the unequality, with the terms of the **[Eq 13]**

$$\lambda k_1 x_1^2 + \lambda k_2 x_1^2 = \lambda x_1^2$$

[Eq 22]

Then, we have in total in the right hand term

$$x_1^2 \lambda(1-\lambda)$$

[Eq 23]

Now, with respect to the **[Eq 10]**, we have in the left hand member

Proposition 2.-The Numerical Reuleaux Method function is **Gateaux differentiable** [**5.2**] for any local minimizer x, that is, if any local minimizer x exists, then, the directional derivative

$$f'(\vec{x},\vec{d}) = \lim_{t\to 0} \frac{f(\vec{x}+t\vec{d}) - f(\vec{x})}{t} \qquad \textbf{[Eq 33]}$$

is linear in $\vec{d} \in E$

in other words $f'(\vec{x},\vec{d}) = \langle \vec{a},\vec{d} \rangle$

for some element, $\vec{a} \in E$

and $\nabla f(\vec{x}) = \vec{a}$

Proof.-We will prove firstly the existence of the directional derivative for a local minimizer $\vec{x}$ and secondly, the linearity

of the directional derivative in *d*. Finally, we will show that $\nabla f(\vec{x}) = \vec{a}$.

For the simple model of the **[Fig 2]**, but choosing two Cartesian coordinates, **X** and **Y**, we obtain

$\vec{x}_1 = (x_1, y_1)^t$

$\vec{x}_2 = (x_2, y_2)^t$

$then$

$f(\vec{x}) = k_1[(x-x_1)^2 + (y-y_1)^2] + k_2[(x-x_2)^2 + (y-y_2)^2]$

and

$\nabla f(\vec{x}) = [2k_1(x-x_1) + 2k_2(x-x_2), 2k_1(y-y_1) + 2k_2(y-y_2)]^t$

$therefore$

$f(\vec{x} + t\,\vec{d}) = f(x + td_x, y + td_y)$

$derivative$:

$$f'(\vec{x},\vec{d}) = lim_{t\to 0} \frac{k_1[(x+td_x-x_1)^2 + (y+td_y-y_1)^2] + k_2[(x+td_x-x_2)^2 + (y+td_y-y_2)^2]}{t} -$$
$$- \frac{k_1[(x-x_1)^2 + (y-y_1)^2] + k_2[(x-x_2)^2 + (y-y_2)^2]}{t} \qquad \textbf{[Eq 34]}$$

The calculation of this derivative has to be carried out by L'Hopital rule, and we obtain finally

$$f'(\vec{x},\vec{d}) = k_1 2d_x(x-x_1) + k_1 2d_y(y-y_1) + k_2 2d_x(x-x_2) + k_2 2d_y(y-y_2) =$$
$$= [2k_1(x-x_1) + 2k_2(x-x_2), 2k_1((y-y_1) + 2k_2(y-y_2)] \times [d_x, d_y]^t = \langle \vec{a},\vec{d} \rangle \qquad \textbf{[Eq 35]}$$

Therefore, the directional derivative exists, and is linear in d, as it is shown in **[Eq 35]**. Besides, according to the statement of the **[Eq 34]**, we have

$$\vec{a} = \nabla f(\vec{x}) = [2k_1(x-x_1) + 2k_2(x-x_2), 2k_1(y-y_1) + 2k_2(y-y_2)]^t$$
$$and$$
$$\vec{d} = (d_x, d_y)^t \qquad \textbf{[Eq 36]}$$

In consequence, the **Proposition 2** is proven. What has been show, until now, is that the Numerical Reuleaux Method is a convex function, Gateaux differentiable, and has local minima. In the following, it will be shown that the objective function of the model is a differentiable function, has local minima, and a global minimum. There are different methods to demonstrate these points, and the most simple and easiest to understand have been chosen.

3.3-Frechet Differentiability

This mathematical property is stricter than **Gateaux Differentiability** [**5.2**]. The concept of this condition is that, when we are approaching the Minimum (or Global Minimum, it depends of the particular problem) of the Objective Function, we can choose any arbitrary direction. Therefore, accomplished this condition, the feasibility to catch up the Minimum is higher than the **Gateaux Differentiability** process. We set the following **Proposition 3**,

Proposition 3.-The **NRM** Objective Function (**f**) is **Frechet Differentiable**, namely,

Given the function **f** (**NRM** Objective Function), differentiable and continuous, with

$$\emptyset = \nabla f(\vec{x}) \qquad \textbf{[Eq 37]}$$

the limit, such as,

$$\lim_{\vec{x} \to \vec{y}} \frac{f(\vec{y}) - f(\vec{x}) - (\emptyset, \vec{y} - \vec{x})}{\|\vec{y} - \vec{x}\|} \to 0 \qquad \textbf{[Eq 38]}$$

tends to zero for any $\vec{x}$, $\vec{y}$, nearby the Global Minimum.

Proof

f is differentiable and continuous as we proved in **Proposition 2**, now, we will approach $\vec{x}$ towards $\vec{y}$ through straight lines, such as

if $\vec{x} = (x_1, x_2)$

and $\vec{y} = (y_1, y_2)$

suppose that when we are approaching with straight lines, we can find some real numbers **h**, **k**, such as,

$$y_1 - h = x_1 \quad h \in R^1$$
$$y_2 - k = x_2 \quad k \in R^1$$

that is,

$$\vec{y} = \begin{pmatrix} y_1 - h \\ y_2 - k \end{pmatrix} = \begin{pmatrix} x_1 \\ x_2 \end{pmatrix} = \vec{x}$$

and we make with this approximation a Taylor series in **2D**,

$$f(\vec{y}) = f(\vec{x}) + \left(h\frac{\partial}{\partial x_1} + k\frac{\partial}{\partial x_2}\right) \times f(\vec{x}) + \frac{1}{2!}\left(h\frac{\partial}{\partial x_1} + k\frac{\partial}{\partial x_2}\right)^2 \times f(\vec{x}) + ..$$

[Eq 39]

now we pass on the left side the first two terms of the right side,

$$f(\vec{y}) - f(\vec{x}) - \left(h\frac{\partial}{\partial x_1} + k\frac{\partial}{\partial x_2}\right) \times f(\vec{x}) = \frac{1}{2!}\left(h\frac{\partial}{\partial x_1} + k\frac{\partial}{\partial x_2}\right)^2 \times f(\vec{x}) + ..$$

[Eq 40]

the left part is just the numerator of the limit-fraction of the **Proposition 3**, that is, we can see the last term of the numerator identity better as follows,

$$\langle \emptyset, \vec{y} - \vec{x} \rangle = \langle \nabla f(\vec{x}), \vec{y} - \vec{x} \rangle = h\frac{\partial f(\vec{x})}{\partial x_1} + k\frac{\partial f(\vec{x})}{\partial x_2}$$

[Eq 41]

now we show that the first term on the right part tends to 0 when **h** and **k** tend both to 0, and it follows straightforward that the rest of the Taylor terms with higher powers tend also to zero quickly,
so we have,

$$\lim_{\vec{x}\to\vec{y}} \frac{f(\vec{y}) - f(\vec{x}) - \langle \emptyset, \vec{y} - \vec{x} \rangle}{\|\vec{y} - \vec{x}\|} = \lim_{\substack{h\to 0 \\ k\to 0}} \frac{f(\vec{y}) - f(\vec{x}) - \langle \emptyset, \vec{y} - \vec{x} \rangle}{\|\vec{y} - \vec{x}\|} = \lim_{\substack{h\to 0 \\ k\to 0}} \frac{\frac{1}{2!}\left(h\frac{\partial}{\partial x_1} + k\frac{\partial}{\partial x_2}\right)^2 \times f(\vec{x}) + ..}{\|\vec{y} - \vec{x}\|} =$$

$$\lim_{\substack{h\to 0 \\ k\to 0}} \frac{\frac{1}{2!}\left(h\frac{\partial}{\partial x_1} + k\frac{\partial}{\partial x_2}\right)^2 \times f(\vec{x}) + ..}{(h^2 + k^2)^{1/2}} = \text{(we omit the rest of the summatory +…. for the sake of simplicity)}$$

=

$$= \lim_{\substack{h\to 0 \\ k\to 0}} \frac{\frac{1}{2!}\left(h\frac{\partial}{\partial x_1}\right)^2 \times f(\vec{x}) + \frac{1}{2!}\left(k\frac{\partial}{\partial x_2}\right)^2 \times f(\vec{x}) + \left(h\frac{\partial}{\partial x_1}\right) \times \left(k\frac{\partial}{\partial x_2}\right) \times f(\vec{x})}{(h^2 + k^2)^{1/2}} =$$

we are interested on the real factors **h** and **k**,

$$= \lim_{\substack{h\to 0 \\ k\to 0}} \frac{\frac{1}{2!}h^2\left(\frac{\partial}{\partial x_1}\right)^2 + \frac{1}{2!}k^2\left(\frac{\partial}{\partial x_2}\right)^2 + hk\left(\frac{\partial}{\partial x_1}\right) \times \left(\frac{\partial}{\partial x_2}\right)}{(h^2 + k^2)^{1/2}} \times f(\vec{x}) =$$

to simplify, we work in polar coordinates, such as,

$$h = r\,sin\theta$$

$$k = r\,cos\theta$$

hence, for any value of **θ**,

$$= \lim_{r\to 0} \frac{\frac{1}{2!}(rsin\theta)^2\left(\frac{\partial}{\partial x_1}\right)^2 + \frac{1}{2!}(rcos\theta)^2\left(\frac{\partial}{\partial x_2}\right)^2 + r^2 sin\theta cos\theta\left(\frac{\partial}{\partial x_1}\right)\times\left(\frac{\partial}{\partial x_2}\right)}{((rsin\theta)^2 + (rcos\theta)^2)^{1/2}} \times f(\vec{x}) =$$

$$= \lim_{r\to 0} \frac{\frac{1}{2!}(rsin\theta)^2\left(\frac{\partial}{\partial x_1}\right)^2 + \frac{1}{2!}(rcos\theta)^2\left(\frac{\partial}{\partial x_2}\right)^2 + r^2 sin\theta cos\theta\left(\frac{\partial}{\partial x_1}\right)\times\left(\frac{\partial}{\partial x_2}\right)}{r} \times f(\vec{x}) =$$

$$= \lim_{r\to 0} \left[\frac{1}{2!} r(sin\theta)^2\left(\frac{\partial}{\partial x_1}\right)^2 + \frac{1}{2!} r(cos\theta)^2\left(\frac{\partial}{\partial x_2}\right)^2 + r\, sin\theta cos\theta\left(\frac{\partial}{\partial x_1}\right)\times\left(\frac{\partial}{\partial x_2}\right)\right]\times f(\vec{x}) = 0$$

[Eq 42]

for any value of $f(\vec{x})$ *nearby the Global Minimum,* ■

It follows the same for all the Taylor terms of the numerator, as we wanted to demonstrate.

Therefore, **Proposition 3** is proven (more types of demonstrations are also possible).

Note the computational/numerical significance of what we have proven, which is the paper aim in Applied Mathematics. Many optimization algorithms work with derivatives (there are exceptions, the so-called derivative-free Optimization, for instance). If most of the derivatives of the Nonlinear Objective Function are tending to null when approaching to the Global Minimum, it implies that the computational effort will be easy and quick. Therefore, we have demonstrated the smoothness of the optimization process for the Objective Function of the **NRM**.

3.4.-Strict Differentiability

This mathematical property is tougher than **Frechet Differentiability** [**5.2**]. The concept of this condition is that, when we are approaching the Minimum (or Global Minimum, it depends of the particular problem) of the Objective Function, we can choose any two arbitrary directions. Therefore, the feasibility to catch up the Minimum is higher than the **Frechet Differentiability** process. We set the following **Proposition 4**,

Proposition 4.-The **NRM** Objective Function (**f**) is **Strict Differentiable** [**5.2**], namely Given the function **f** (**NRM** Objective Function) differentiable and continuous, with

$$\emptyset = \nabla f(\vec{x})$$

the limit, such as,

$$\lim_{\vec{y},\vec{z}\to\vec{x}} \frac{f(\vec{y}) - f(\vec{z}) - (\emptyset, \vec{y}-\vec{z})}{\|\vec{y}-\vec{z}\|} = 0 \qquad \textbf{[Eq 43]}$$

tends to zero for any $\vec{x}$, $\vec{y}$, $\vec{z}$, nearby the Global Minimum.

Proof

f is Differentiable and Continuous as we proved in **Proposition 2**, and the Proof is just the same than the **Proposition 3**, but we have in this case two vectors approaching to $\vec{x}$

$$\begin{aligned} y_1 - h_1 &= x_1 \quad h_1 \in R^1 \\ y_2 - k_1 &= x_2 \quad k_1 \in R^1 \\ z_1 - h_2 &= x_1 \quad h_2 \in R^1 \\ z_2 - k_2 &= x_2 \quad k_2 \in R^1 \end{aligned}$$

and hence,

$$\begin{aligned} y_1 - z_1 &= h_2 - h_1 \quad h_2 \\ y_2 - z_2 &= k_2 - k_1 \quad k_2 \end{aligned}$$

and the denominator of [**Eq 43**] towards the limit would be

$$\|\vec{y} - \vec{z}\| = (h_2^2 + k_2^2)^{1/2}$$

The reader can carry out the rest of the proof development without any difficulty based in these approximations

Note just the same as in **Proposition 3,** the computational/numerical significance of what we have proven, which is the paper aim in Applied Mathematics. It is happening the same than in **Frechet Differentiability**, but now we approach to the Global Minimum along two any arbitrary directions. This mathematical condition adds more trust upon the Objective Function of the **NRM**.

IV. Mathematical Optimization

In this Section the Existence of a Global Minimum is proven, and we determine the basic analytic formulas (**2D** and **3D**) for the Global Minimum.

4.1.-Existence of Global Minimum

Now we will try to find the analytic Formula for the Global Minimum, both in **2D** and **3D**.

Proposition 5.-The Numerical Reuleaux Method objective function has a unique global minimum

$$\vec{x} \quad with \quad \nabla f(\vec{x}) = 0.$$

Proof.-It was shown in **Proposition 2** the existence of the local minima in the objective function of the model, which is Gateaux differentiable. We will demonstrate that the objective function critical point

$\vec{x} \quad with \quad \nabla f(\vec{x}) = 0.$, such as minimum, and therefore a **Global Minimum**.

The proof is developed in 2D, and can be easily extended for n-dimensions. We start with the first objective function

$$\vec{x}_1 = (x_1, y_1)^t$$
$$\vec{x}_2 = (x_2, y_2)^t$$
$$then$$
$$f(\vec{x}) = k_1[(x - x_1)^2 + (y - y_1)^2] + k_2[(x - x_2)^2 + (y - y_2)^2]$$
$$and$$
$$\nabla f(\vec{x}) = [2k_1(x - x_1) + 2k_2(x - x_2), 2k_1(y - y_1) + 2k_2(y - y_2)]^t = 0$$
$$Hence$$
$$\frac{\partial f(\vec{x})}{\partial x} = 2k_1(x - x_1) + 2k_2(x - x_2) = 0$$
$$\frac{\partial f(\vec{x})}{\partial y} = 2k_1(y - y_1) + 2k_2(y - y_2) = 0$$
$$solutions$$
$$x = k_1 x_1 + k_2 x_2$$
$$and$$
$$y = k_1 y_1 + k_2 y_2 \qquad \textbf{[Eq 44]}$$

Therefore, the critical point solutions are unique, now we will carry out the second derivatives to show that the Hessian is at least a semi-definite positive matrix, and therefore the critical point is a minimum and unique, that is, a global minimum

$$\frac{\partial^2 f(\vec{x})}{\partial x^2} = 2(k_1 + k_2) = 2 \quad > 0$$

and **[Eq 45]**

$$\frac{\partial^2 f(\vec{x})}{\partial y^2} = 2(k_1 + k_2) = 2 \quad > 0$$

Now the second partial derivatives in **X** and **Y**

$$\frac{\partial^2 f(\vec{x})}{\partial x \partial y} = 0$$
$$and$$
$$\frac{\partial^2 f(\vec{x})}{\partial y \partial x} = 0$$
$$Hessian$$
$$Det[Hessian] = Det\begin{pmatrix} \frac{\partial^2 f(\vec{x})}{\partial x^2} & \frac{\partial^2 f(\vec{x})}{\partial x \partial y} \\ \frac{\partial^2 f(\vec{x})}{\partial y \partial x} & \frac{\partial^2 f(\vec{x})}{\partial y^2} \end{pmatrix} = 4 \geq 0$$
$$therefore$$
$$if$$
$$\vec{X} = (x, y, z)^t \in E$$
$$then$$

$2D$

$$(x,y)\times\begin{pmatrix}\frac{\partial^2 f(\vec{x})}{\partial x^2} & \frac{\partial^2 f(\vec{x})}{\partial x\partial y}\\ \frac{\partial^2 f(\vec{x})}{\partial y\partial x} & \frac{\partial^2 f(\vec{x})}{\partial y^2}\end{pmatrix}\times\begin{pmatrix}x\\y\end{pmatrix}=(x,y)\times\begin{pmatrix}2 & 0\\0 & 2\end{pmatrix}\times\begin{pmatrix}x\\y\end{pmatrix}=(2x,2y)\times\begin{pmatrix}x\\y\end{pmatrix}=2x^2+2y^2\geq 0$$

for all $\vec{x}\in E$.

2) [Eqs 46]

In consequence, the proposition is demonstrated. On the whole, we have obtained important practical results about the objective function of the Reuleaux Numerical Model. We have proven that it is Gateaux and Frechet Differentiable, Strict Differentiable, and has a global minimum. This implies that the optimization process to find the Numerical IRC, as said above, will be smooth and mathematically trustful.

3) 4.2.-Global Minimum General Formula, 2D and 3D

Corollary 1.-The general solution for the optimal IRC in the Numerical Reuleaux method for **n** voxels reads,

$$\vec{X}_{optimaln}=\left(\sum_{i=1}^{n}\frac{m_i x_i}{\sum_{j=1}^{n}m_j},\sum_{i=1}^{n}\frac{m_i y_i}{\sum_{j=1}^{n}m_j},\sum_{i=1}^{n}\frac{m_i z_i}{\sum_{j=1}^{n}m_j}\right)^T$$

$$where$$
$$\vec{x}_i=(x_i,0,0)^t$$
$$\vec{y}_i=(0,y_i,0)^t$$
$$\vec{z}_i=(0,0,z_i)^t$$

[Eq 47]

and these are the coordinates for each particular IRC of each voxel **i**.

Proof.-We obtained in **Proposition 7** the solution for the global minimizer for **n=2** (two voxels)

$$\vec{x}_1=(x_1,y_1)^t$$
$$\vec{x}_2=(x_2,y_2)^t$$
$$solutions$$
$$x_{n=2}=k_1x_1+k_2x_2=\sum_{i=1}^{2}k_ix_i=\sum_{i=1}^{2}\frac{m_ix_i}{\sum_{j=1}^{2}m_j}$$
$$and$$
$$y_{n=2}=k_1y_1+k_2y_2=\sum_{i=1}^{2}\frac{m_iy_i}{\sum_{j=1}^{2}m_j}$$
$$since$$

$$k_1 = \frac{m_1}{m_1 + m_2}$$
$$k_2 = \frac{m_2}{m_1 + m_2}$$
$$hence$$
$$\vec{X}_{optimal,n=2} = (\sum_{i=1}^{2} \frac{m_i x_i}{\sum_{j=1}^{2} m_j}, \sum_{i=1}^{2} \frac{m_i y_i}{\sum_{j=1}^{2} m_j})^T$$

[Eq 48]

In the same way, by using the minimization method of **Proposition 7** in **3D**, we could obtain for 3 voxels

$$\vec{X}_{optimal,n=3} = (\sum_{i=1}^{3} \frac{m_i x_i}{\sum_{j=1}^{3} m_j}, \sum_{i=1}^{3} \frac{m_i y_i}{\sum_{j=1}^{3} m_j}, \sum_{i=1}^{3} \frac{m_i z_i}{\sum_{j=1}^{3} m_j})^T$$

[Eq 49]

Now we can write the general formula for **n** voxels in **3D**, namely

$$\vec{X}_{optimal,n} = (\sum_{i=1}^{n} \frac{m_i x_i}{\sum_{j=1}^{n} m_j}, \sum_{i=1}^{n} \frac{m_i y_i}{\sum_{j=1}^{n} m_j}, \sum_{i=1}^{n} \frac{m_i z_i}{\sum_{j=1}^{n} m_j})^T$$

[Eq 50]

All in all, these obtained formulas **[Eq 40]** to **[Eq 43]** are similar to the Classic Mechanics Theory of the Mass Center determination. We could observe some kind of parallelism between the Mass Center Equations and the Numerical Reuleaux Method optimal solutions. We note that this analytic solution for the optimization problem is very easy to compute, and therefore the saved computational time is significant. It is not necessary to carry out any optimization program for the general objective function, since it suffices to calculate directly the analytic solution. However, this analytic solution is based on constant density distributions for each voxel. On the other hand, it is more convenient reformulate **[Eq 43]** in a matrix equation, such as,

$$\vec{X}_{optimal,n} = \begin{pmatrix} x_{optimal} \\ y_{optimal} \\ z_{optimal} \end{pmatrix} = \begin{pmatrix} x_1 & x_2 & \cdot & x_n \\ y_1 & y_2 & \cdot & y_n \\ x_1 & z_2 & \cdot & z_n \end{pmatrix} \times \begin{pmatrix} k_1 \\ k_2 \\ \cdot \\ k_n \end{pmatrix}$$
$$(3,1) = (3, N) \times (N, 1)$$
$$or$$
$$\vec{X}_{optimal} = [A] \times \vec{K}$$

[Eq 51]

where K is the matrix that contains the weight factors for each voxel.

V. Errors Boundaries and Error Reduction Techniques

In this Section the most important Error and its corresponding boundaries are defined and calculated. The Voxel-Volume error is related to volume variations of each voxel during the **PRB** movement. We develop all these mathematical properties through **Theorems 2**,**3**, and **Corollary 2**.

5.1.-Voxel-Volume Error

Theorem 2.-If the Numerical Reuleaux Method is applied on the dynamics of a rectangular pseudo-rigid body, the mathematical weight error of this least squares model **[Eq 5.1]**, decreases proportionally to the reduction of the voxels dimensions.

Proof.-The demonstration is based on the fact that the weight factors of the objective function in the least squares model,
[Eq 5.1], decrease when the voxel dimensions become smaller.
We had the objective function

$$f(\vec{x}) = \sum_{i=1}^{n} \frac{\int_{V_i} \rho_i(\vec{x_i}) dv}{\sum_{j=1}^{n} \int_{V_j} \rho_j(\vec{x_j}) dv_j} \times \left\| \vec{x} - \vec{x_i} \right\|^2 \qquad \textbf{[Eq 52]}$$

For the sake of simplicity, we take the integral weight factors in only two dimensions, and the third dimension is constant, **k**. Therefore, we have the following masses

$$m_i = \int_{V_i} k\rho_i(x,y) dv_i = \int_{V_i} k\rho_i\,(x,y) dx_i dy_i \qquad \textbf{[Eq 53]}$$

written in a simpler form, for a voxel of dimensions (a,b,k)

$$m = \int_0^a \int_0^b k\rho(x,y) dx dy = m(x,y) \qquad \textbf{[Eq 54]}$$

This is an integral function of two variables, whose expression is an integral equation. Therefore, to carry out the calculation of the errors, it is necessary to derivate under the integral sign, as follows

$$\boldsymbol{\frac{\partial m}{\partial x} = \int_0^a \int_0^b k \frac{\partial(x,y)}{\partial x} dy dx + \int_0^b k\rho(a,y) dy - \int_0^b k\rho(0,y) dy} \qquad \textbf{[Eq 55]}$$

$$\frac{\partial m}{\partial y} = \int_0^a \int_0^b k \frac{\partial(x,y)}{\partial y} dy dx + \int_0^a k\rho(x,b) dx - \int_0^a k\rho(x,0) dx \qquad \textbf{[Eq 56]}$$

Therefore, the total error of the mass is,

$$\varepsilon_m = \sqrt{\left(\frac{\partial m}{\partial y}\right)^2 \varepsilon_y^2 + \left(\frac{\partial m}{\partial x}\right)^2 \varepsilon_x^2}$$

[Eq 57]

where ε_x and ε_y are constants that depend of the measurement precision of the system (relative errors), whose values are the same independently of the size of the voxel.

$$\left(\frac{\partial m}{\partial x}\right)^2 \varepsilon_x^2 \to 0$$

$$\left(\frac{\partial m}{\partial y}\right)^2 \varepsilon_y^2 \to 0$$

Now we will prove that when a,b $\to 0$, both factors

[Eq 58]

We need now to develop the integral of the **[Eq 55]** in numerical series by Gauss method, because it is only sufficient to demonstrate the Theorem for this term of **[Eq 57].** Therefore, it is only necessary to demonstrate this for $\left(\frac{\partial m}{\partial x}\right)^2 \varepsilon_x^2$ The first term of, $\frac{\partial m}{\partial x}$ according to **[Eq 55]** is

$$\int_0^a \int_0^b k \frac{\partial(x,y)}{\partial x} dydx \cong \sum_{x_i=0}^{x_i=a} \sum_{y_i=0}^{y_i=b} k \times \left[\frac{\partial(x,y)}{\partial x}\right]_{x_i,y_i} \Delta y \Delta x \to_{a,b\to 0} 0 \qquad \textbf{[Eq 59]}$$

where we have divided the intervals **[0,a]** and **[0,b]** of the voxel into small subvoxels whose individual sizes are **kΔxΔy**. For example, we divide the intervals into **m** divisions such as

$$\Delta x = \frac{a}{m}$$
$$\Delta y = \frac{b}{m} \qquad \textbf{[Eq 60]}$$

Therefore, the second term would be

$$\int_0^b k\rho(a,y)dy \cong \sum_{y_i=0}^{y_i=b} k \times [\rho(a,y)]_{y_i} \Delta y \to_{b\to 0} 0 \qquad \textbf{[Eq 61]}$$

And the third term approximation is

$$-\int_0^b k\rho(0,y)dy \cong -\sum_{y_i=0}^{y_i=b} k \times [\rho(0,y)]_{y_i} \Delta y \to_{b\to 0} 0 \qquad \textbf{[Eq 62]}$$

Therefore, these terms tend to zero when the dimensions of the voxels decrease, in particular the first term of the equation
[Eq 58]. In consequence, the Theorem is proven.

5.2.-Voxel-Volume Error Boundaries

This error type is more related to the Second Objective Function. We set the bounds for this error through **Theorem 3**.

Theorem 3.-If the Numerical Reuleaux Method is applied on, the error due to the voxels size shows lower superior bounds, when the voxels size decreases. In other words, the smaller voxels, the smaller volume-variation errors.

Proof.-This theorem is understood intuitively, because the smaller voxels size, the nearer is the natural approximation to a particules system. However, it is necessary to prove it mathematically and carry out useful superior bounds and quantifications of the error values.
This demonstration has two parts. The first deals with the proofs related to the numerical determination of the superior bounds of the error corresponding to any voxel size. The second shows that these bounds decrease when the the voxel size decreases its volume. Therefore, according to [**Fig 6**], we have a coordinates system in 2D, **X**, **Y**, that gives the vector

position of the IRC when the body is rigid, that is, $\overrightarrow{Xexact}$ or $\overrightarrow{X_a^{\omega}}$ $\overrightarrow{Xe}$, and the IRC position for the pseudo-rigid for the pseudo-rigid body, that is,

$\overrightarrow{X\ approximated}$, or $\overrightarrow{Xa}$. The angle **θ**, [**Fig 6**], is the same for the perpendicular Reuleaux segments, just because those

segments are perpendicular to the Reuleaux segments that define this angle **θ**. The Reuleaux segments, as in previous demonstrations, are AA', and the distance AA'', so we see that when

$$\boldsymbol{\theta \to 0}$$
$$\boldsymbol{then}$$
$$\boldsymbol{A'' \to A'}$$
$$\boldsymbol{if}$$
$$\boldsymbol{h = A'A''}$$
$$\boldsymbol{then}$$
$$\boldsymbol{h \to 0}$$

[Eq 63]

We also define, in [**Fig 6**]

$$\vec{d} = \vec{x}_a - \vec{x}_e$$

[Eq 64]

If we take the weight factor, in the objective function part of [**Eq 4**], as a constant **k**, for the sake of simplicity

$$f(\vec{x}) = k \times \left\|\vec{x} - \vec{x}_e\right\|^2 = k \times \left\|\vec{x}_e - \vec{x}\right\|^2 = k \times \left\|(\vec{x} - \vec{x}_a) + (\vec{x}_a - \vec{x}_e)\right\|^2 \leq$$
$$k \times \left\|\vec{x} - \vec{x}_a\right\|^2 + k \times \left\|\vec{x}_e - \vec{x}_a\right\|^2 + 2k \times \left\|\vec{x} - \vec{x}_a\right\| \times \left\|\vec{x}_e - \vec{x}_a\right\| =$$
$$= k \times \left\|\vec{x}_e - \vec{x}_a\right\|^2 + k \times \left\|\vec{x} - \vec{x}_a\right\| \times \left[\left\|\vec{x} - \vec{x}_a\right\| + 2 \times \left\|\vec{x}_e - \vec{x}_a\right\|\right]$$

[Eq 65]

In conclusion, from the [**Eq 64**] development, we have

$$f(\vec{x}) \leq k \times \left\|\vec{x}_e - \vec{x}_a\right\|^2 + k \times \left\|\vec{x} - \vec{x}_a\right\| \times \left[\left\|\vec{x} - \vec{x}_a\right\| + 2 \times \left\|\vec{x}_e - \vec{x}_a\right\|\right] \qquad \textbf{[Eq 66]}$$

Now, we are interested in the variation of the objective function $f(x)$ with respect to the distance that defines the difference between the IRC approximated $\vec{X}_a$, and the IRC exact, $\vec{X}_e$. Then we call

$$\varepsilon = \left\|\vec{X}_e - \vec{X}_a\right\|$$
$$so$$
$$\frac{\partial f(\vec{x})}{\partial \varepsilon} \leq 2k\varepsilon + 2k \times \left\|\vec{x} - \vec{x}_a\right\|$$

[Eq 67]

Therefore, since we are working in 2D, the volume error respect to **ε** will be

$$\varepsilon_V = \sqrt{\left(\frac{\partial f(\vec{x})}{\partial \varepsilon}\right)^2 (\varepsilon_y^2 + \varepsilon_x^2)}$$

[Eq 68]

Because it is necessary to sum the relative errors of **X** and **Y**, since the distance **ε** depends on those two variables. Then, we have

$$\varepsilon_V = \sqrt{\left(\frac{\partial f(\vec{x})}{\partial \varepsilon}\right)^2 (\varepsilon_y^2 + \varepsilon_x^2)} \leq 2k \times (\varepsilon + \left\|\vec{x} - \vec{x}_a\right\|) \times (\varepsilon_x^2 + \varepsilon_y^2)^{1/2} \leq$$
$$\leq 2k \times (\varepsilon + \left\|\vec{x} - \vec{x}_a\right\|) \times (\varepsilon_x^2 + \varepsilon_y^2 + 2\varepsilon_x\varepsilon_y)^{1/2} = 2k \times (\varepsilon + \left\|\vec{x} - \vec{x}_a\right\|) \times (\varepsilon_x + \varepsilon_y)$$
$$then$$

$$\boxed{\varepsilon_V \leq 2k \times (\varepsilon + \left\|\vec{x} - \vec{x}_a\right\|) \times (\varepsilon_x + \varepsilon_y)}$$

[Eq 69]

Here, [**Eq 69**], it is seen that the bounds of the volume error depend on two factors, apart of the weight ones and the relative errors constants for each dimension, $\mathcal{E}_x$ and $\mathcal{E}_y$. The first is the difference between the **exact IRC** and the **approximated IRC**, **ε**, which is linear. The second depends of the difference between the **approximated IRC** (the corresponding to the completely rigid body) and the coordinates of the **optimal IRC** for the whole group of voxels. This value will be shown that depends on the number of voxels. That is, when the number of voxels increases, the distance between the cloud of distribution of IRCs points for the voxels, and the **approximated IRC** decreases. As a result, the distance between the **optimal IRC** and the **approximated IRC** decreases.

Now we will show the second part of the **Theorem 3**, that is, when the voxels size decreases, the bounds of ε_V become
smaller. Suppose that the superior voxel of the **[Fig 6]** is divided into two smaller voxels, according to **[Fig 7]**. We set a 2D

Cartesian coordinates system, **X**, **Y**, and find the position vectors for each IRC exact,

$\overrightarrow{X_{e1}}$

and $\vec{X}_{e2}$

($\mathbf{e_1}$ for the upper voxel, and $\mathbf{e_2}$ for the lower voxel). Let's call now

$\overrightarrow{X_{e3}}$ the IRC corresponding to the sum of voxels 1 and voxel 2 in **[Fig 7]**
(in **[Fig 6]** is

$\overrightarrow{X_e}$), and $\overrightarrow{X_a}$ the position vector for the IRC also for the sum of voxel 1 and voxel 2 (in **[Fig 6]**, is $\vec{X}_a$, it is
just the same). As it is seen and guessed in **[Fig 7]**, there is a number of inequal distances such as

$$\varepsilon_1 = \left\| \vec{X}_{e1} - \vec{X}_a \right\| \leq \varepsilon_3 = \left\| \vec{X}_{e3} - \vec{X}_a \right\|$$
$$and$$
$$\varepsilon_2 = \left\| \vec{X}_{e2} - \vec{X}_a \right\| \leq \varepsilon_3 = \left\| \vec{X}_{e3} - \vec{X}_a \right\|$$
$$with$$
$$m = m_1 + m_2$$

[Eq 70]

where m is the resultant weight factor (mass) of the sum of voxel 1 and voxel 2 weight factors (masses). Then we will show that in the objective function corresponding to two voxels, the bounds are lower than the objective function for one voxel. For economy of writing, the weight factors are **m**, $\mathbf{m_1}$, and $\mathbf{m_2}$, so we have

$$\varepsilon_{V-for-two-voxels} \leq 2m_1 \times (\varepsilon_1 + \left\| \vec{x} - \vec{x}_a \right\|) \times (\varepsilon_x + \varepsilon_y) + 2m_2 \times (\varepsilon_2 + \left\| \vec{x} - \vec{x}_a \right\|) \times (\varepsilon_x + \varepsilon_y)$$

[Eq 71]

Now, we suppose that we have found an optimal IRC point, such as

$$\vec{X}^*_{for-voxel1-and-voxel2} = \vec{X}^*_2$$

So we get

$$\varepsilon_{V-for-two-voxels} \leq 2m_1 \times (\varepsilon_1 + \left\| \vec{x}^*_2 - \vec{x}_a \right\|) \times (\varepsilon_x + \varepsilon_y) + 2m_2 \times (\varepsilon_2 + \left\| \vec{x}^*_2 - \vec{x}_a \right\|) \times (\varepsilon_x + \varepsilon_y)$$

[Eq 72]

And we start to carry on the development of the inequalities

$$\varepsilon_{V-for-two-voxels} \leq 2m_1 \times (\varepsilon_1 + \left\| \vec{x}^{\,*}_2 - \vec{x}_a \right\|) \times (\varepsilon_x + \varepsilon_y) + 2m_2 \times (\varepsilon_2 + \left\| \vec{x}^{\,*}_2 - \vec{x}_a \right\|) \times (\varepsilon_x + \varepsilon_y)$$

$$\leq$$

$$\leq 2m_1 \times (\varepsilon_3 + \left\| \vec{x}^{\,*}_2 - \vec{x}_a \right\|) \times (\varepsilon_x + \varepsilon_y) + 2m_2 \times (\varepsilon_3 + \left\| \vec{x}^{\,*}_2 - \vec{x}_a \right\|) \times (\varepsilon_x + \varepsilon_y)$$

[Eq 73]

Then we continue with the development of the inequality of **[Eq 73]**

$$\varepsilon_{V-for-two-voxels} \leq 2m_1 \times (\varepsilon_3 + \left\| \vec{x}^{\,*}_2 - \vec{x}_a \right\|) \times (\varepsilon_x + \varepsilon_y) + 2m_2 \times (\varepsilon_3 + \left\| \vec{x}^{\,*}_2 - \vec{x}_a \right\|) \times (\varepsilon_x + \varepsilon_y)$$

$$\leq$$

$$\leq 2m_1 \times (\varepsilon_3 + \left\| \vec{x}^{\,*}_2 - \vec{x}_a \right\|) \times (\varepsilon_x + \varepsilon_y) + 2m_2 \times (\varepsilon_3 + \left\| \vec{x}^{\,*}_2 - \vec{x}_a \right\|) \times (\varepsilon_x + \varepsilon_y) \leq$$

$$\leq \left[(\varepsilon_3 + \left\| \vec{x}^{\,*}_2 - \vec{x}_a \right\|) \times (\varepsilon_x + \varepsilon_y) \right] \times (2m_1 + 2m_2) = \left[(\varepsilon_3 + \left\| \vec{x}^{\,*}_2 - \vec{x}_a \right\|) \times (\varepsilon_x + \varepsilon_y) \right] \times 2m$$

[Eq 74]

According to **[Eq 70]**. Now, we consider that the optimal point (for the two voxels that result from the division of the voxel of **[Fig 7]**),

$\vec{X}^{**}_2$, is obviously nearer from voxel 1 and voxel 2 ICRs respectively, than the **optimal IRC** for the sum of these

two voxels, which in this case coincides with the coordinates of the 2). Then

$\vec{X}_{e3}$ (because there is only one voxel = voxel 1 + voxel

$$\vec{X}_{e3} = \vec{X}^{\,*}_{for-one-voxel} = \vec{X}_1$$

Therefore, we have

$$\left\| \vec{X}^{\,*}_2 - \vec{X}_a \right\| \leq \left\| \vec{X}^{\,*}_1 - \vec{X}_a \right\|$$

[Eq 75]

We apply this inequality on **[Eq 74]** in this way

$$\varepsilon_{V-for-two-voxels} \leq \left[(\varepsilon_3 + \left\| \vec{x}^{\,*}_2 - \vec{x}_a \right\|) \times (\varepsilon_x + \varepsilon_y) \right] \times 2m \leq \left[(\varepsilon_3 + \left\| \vec{x}^{\,*}_1 - \vec{x}_a \right\|) \times (\varepsilon_x + \varepsilon_y) \right] \times 2m$$

$$=$$

$$= \varepsilon_{V-for-one-voxel}$$

namely

$$\varepsilon_{V-for-two-voxels} \leq \varepsilon_{V-for-one-voxel}$$

[Eq 76]

In consequence, the second part of the **Theorem 3** is proven, and the complete **Theorem 3** demonstrated. We have now the certainty that the smaller voxels size, the smaller magnitude of errors, and also it has been calculated some approximated upper bounds for the errors.

Till now, we have developed the formula of volume errors for a small number of voxels. Now, it corresponds to a corollary to show the general formula for **N** voxels. It is an interesting fact, as it has been proven, that the longer number of voxels, the smaller distance between the **Optimal IRC** and the **Approximated IRC**, which is another factor that determines the upper bound of the volume error value.

All in all, what has been proven is the optimization convexity of the model, its smoothness, and uniqueness of solution. Additionally, the mathematical function of the model is continuous and Gateaux, Frechet, and Strict differentiable. Therefore, the IRC Numerical Reuleaux Method constitutes an acceptable theoretical frame to carry out an approximation for the determination of a pseudo-rigid body IRC.

The simulations and experimental work constitute also an essential part for this model, and although there would be more theoretical points and properties to be developed and demonstrated in future, it has been checked enough all this theory to pass on the practical matters directly.

5.3.-General Voxel-Volume Error Boundaries

Now we get the General Formula for the Voxel-Volume error Boundaries through the **Corollary 2.**

Corollary 2.-The boundaries for the volume error in the Numerical Reuleaux Method for IRC determination in 2D read

$$\varepsilon_{V-total} = \sum_{i=1}^{N} 2k_i \times (\varepsilon_i + \left\| \vec{x} - \vec{x}_a \right\|) \times (\varepsilon_x + \varepsilon_y)$$

or

$$\varepsilon_{V-total} = \sum_{i=1}^{N} \frac{m_i}{\sum_{j=1}^{N} m_j} \times (\varepsilon_i + \left\| \vec{x} - \vec{x}_a \right\|) \times (\varepsilon_x + \varepsilon_y)$$

where

$\varepsilon_i = \left\| \vec{X}_{ei} - \vec{X}_a \right\|$ for each voxel

[Eq 78]

Proof.-It is only necessary to see that the exact $\vec{X}_{ei}$ is different for each voxel, and this reason determined the IRC vector, different values in every ε_{yi} . Therefore, the total error boundary will be a sum, and the mass weight factors are expressed in the same sum form. We can also show the weight factors in an integral form, by using the notation of **[Eq 5.1]**.

VI. Computational Simulations

For the sake of simplicity, we divide the simulations trials into two groups, namely, **2D** and **3D**. The first one is substantially less complicated than the second for a number of reasons. When the **NRM** is applied on, the mathematical development into the computing program involves the finding of the solution of a linear equations system through the inversion of a matrix, which is 2x2 in **2D**, and 3x3 in **3D**. The Algebraic development of the software in **2D** is therefore simpler, and the inversion of the matrix becomes less difficult and more accurate, since it is less frequent, under random simulations conditions, that this matrix could be singular. The **3D** simulations show more technical difficulties, not only for the 3x3 matrix, but also for the longer number of sentences into the program. In addition, when working in **3D** with a solid whose geometry changes during the movement, it is crucial the selection of the meshing of the pseudo-rigid body to form suitable geometrical groups of the three Reuleaux segments. They originate planes whose intersection could not occur when they are almost parallel [**Subsection 6.4**]. This fact yields to obtain a singular and/or almost singular group of ill-posed matrices into the program, which is rather complicated and inconvenient. Several linear algebraic methods to overcome this difficulty in **3D** are explained clearly in this section. For this purpose, there are some brief examples about the geometrical meshing choice, and programming techniques are detailed with a synthesis of the code that has been used for **2D** Simulations (1 Voxel). The appropriate selection of the meshing for the Reuleaux segments is crucial, mostly in **3D**, to avoid parallelism in the planes intersections. Therefore, this suitable geometrical choice yields to overcome the possibility to obtain in the running program high error values increments for low random deformation changes, and/or singular matrices. Finally, we can assert that there is a clear difference of Error (≈**10%**) between 1 Voxel **3D** and 2 Voxels **3D** [**Tables 4,5**]. This implies that these primary Simulations attemps are supporting the initial theoretical calculations.

6.1.-Basic Mechanics Geometry

We introduce here some basic geometrical ideas to make easy understand the following **Subsection 6.2** of Error Determination Techniques. There are two Fundamental-Basic Theorems and one Remark to catch up the basic concepts and results of this paper,

Basic Theorem 1.-(Extensively demonstrated in Classical Mechanics [**1.1**]).-The position of a solid body can be determined at any time instant by two unique points of the body in **2D**, and three points in **3D**.

Basic Theorem 2.-(Extensively demonstrated in Classical Mechanics [**1.1**]).-Any arbitrary movement in **2D** or **3D** is composed by a translation and a rotation.

Therefore, according to **Theorem 2**, the Reuleaux Point defines the Instantaneous Center of Rotation of the rigid or pseudo- rigid body. The vector that joins the Reuleaux Point with the Coordinates Origin corresponds to the translation vector of the movement.

Remark.-The Reuleaux Method gives a unique solution when the movement is pure in **3D**. That is, there are coordinates variations in the three axes. When the movement is performed into a plane, the Reuleaux Method solution is an axis of Rotation (the movement is really in **2D**).

The significance of these Basic Theorems is that we have a simulated movement wich can be decomposed into a translation and a rotation. The rotation is around the IRC calculated through the **NRM**, and the translation is the distance from the Coordinates Center to that IRC. Therefore, to avoid higher error values when optimizing the rotation matrix, we have to carry out an inverse translation of the **PRB** to the Coordinates Center. This translation is made resting to all the **PRB** points the IRC point coordinates. With this information, it is easy to understand the following **Subsection 6.2**.

6.2.-Error Determination Techniques

The calculations of Errors are given by the classical RMS numerical formulas [**13**,**14**,**20**,**27**,**29**,**36**,**40**]. The method that has been implemented has the following steps, namely,

1.-Calculation of the Approximated Reuleaux Point (Approximated Instantaneous Center of Rotation). This determination is geometrical, and takes a series of geometrical steps (with one or two voxels in this case, and using the computing program [**Subsection 6.5**]. We will denote this point as P_R .

2.-Translation of the Initial true Points (P_1), and Final true Points (P_2), around the Coordinates Origin. Then, we calculate the optimal Rotation Matrix A. The steps are as follows,

Given,

P_R : Reuleaux Point .

P_1 : *Initial Points Matrix*.

P_2 : *Final Points Matrix*.

Find the Matrix A, *such as*,

$A \times (P_1 - P_R) = (P_2 - P_R)$

This matrix A is optimized with Matlab Optimization Toolbox (**MOT**), and its elements are determined. To calculate the RMS Error values, the steps are the following,

Given,

$A_{Approximated}$,

we calculate,

$A_{Approximated} \times (P_1 - P_R)$ $P_{2\ Approximated\ at\ Origin}$ (*we call it* P_{20})

Now, *we translate the approximated points from the Origin to the initial position*,

$P_{2\ Approximated} = P_{20} + P_R$

where N is the Points Number.

The RMS Error value will be,

$$\left\| \frac{(P_2)_{True} - (P_2)_{Approximated}}{N^{1/2}} \right\| \qquad \textbf{[Eq 77]}$$

This Error value corresponds to the Average Quadratic Error for 2 (X,Y) variables in **2D**, and three variables (X,Y,Z) in **3D**. We have not calculated the independent error value for each variable. Finally, the **2D** and **3D** pseudo-orthogonal matrices of the rotation around the IRC are defined.
The Optimized Matrix in **2D** Formula reads,

$$A_{2D} = \begin{pmatrix} A & -B \\ B & A \end{pmatrix} \qquad \textbf{[Eq 78]}$$

The Optimized Matrix in **3D** Formula reads,

$$A_{3D} = \begin{pmatrix} a(1) & a(2) & a(3) \\ a(4) & a(5) & a(6) \\ a(7) & a(8) & a(9) \end{pmatrix} \qquad \textbf{[Eq 79]}$$

6.3.-2D Simulations Results

In these Tables Subsection, a synthesis of 2-10 **2D** Simulations for 1 and 2 voxels is shown. It is seen clearly the difference of Error between 1 and 2 voxels. This Subsection comprises a sufficient amount of numerical data in the Tables where it is possible to check the initial simulations results and carry out the most convenient comparisons. In **Fig 8** it is displayed a basic scheme of the random changes of shape that have been carried out for the simulations.

6.4.-3D Simulations Results [Numerical Data at Appendices]

In these Tables Subsection, a synthesis of 11 **3D** Simulations for 1 and 2 voxels is shown. It is seen clearly the difference of Error between 1 and 2 voxels. This Subsection comprises a sufficient amount of numerical data in the **Tables 4**,**5**, where it is possible to check the initial simulations results and carry out the most convenient comparisons. In **Fig 9** it is displayed a basic scheme of the random changes of shape that have been carried out for the simulations.

6.5.-Software Details, Algebraic Techniques, and Geometrical Meshing Approximations

In **Figure 10**, we display a basic Matlab program used for random Simulations in **2D** [**19**,**43**]. The program starts with a variation of the coordinates X and Y of the final position of the **PRB**. The body of the programs deals with algebraic and geometrical calculations to find out the intersection point of the perpendiculars to the Reuleaux segments at their middle points. The primary structure of the code is simple, although it becomes rather long when the number of voxels increases, and the **PRB** movement is in **3D**. This is the simplest Program, but the software used in these calculations was rather more complicated because of refinement and error reductions methods.
An important technical problem that arose in the **3D** Simulations, was the correct selection of the Reuleaux points of the **PRB** to trace the Reuleaux segments that join the inital position with the final one. The reason is that this geometrical choice, if not selected correctly, can create a parallelism among the planes which are perpendicular to the Reuleaux segments middle points. If so, the consequence would be one or several singular matrices into de computing program.

Therefore, the choice of the geometrical meshing to overcome this difficulty, is to try to select the points meshing in different planes, avoiding as much as possible the coincidence of one or more coordinates [**8**,**15.2**]. In other words, to select as much geometrical variety as possible in **3D**.
But in case that the previous problem is not conveniently set, there is a number of numerical and computational solutions to cope with this difficulty. When a linear system is almost Ill-posed or rather Ill-posed, we can try, among many other options, a LU or QR Factorization, the Jacobi Method, the Gauss-Seidel Method, the Basic Power Method, and others [**19**,**21**,**36**]. On the whole, there is a wide range of possibilities to resolve this computational/numerical challenge [**13**,**27**].

6.6.-A Monte-Carlo Method Overview

When the **PRB** is rather large, the computational work could become inmense, if working with a high number of voxels. In this case, a Theoretical Monte-Carlo Algorithm has been designed to overcome this technical difficulty [**10**,**31**]. When using Monte-Carlo, we only have to determine the approximated IRC for a random number of voxels, and set the desired tolerance into the program. The reader can obtain information about this simple algorithm, which still can be refined and improved [**10**,**31**] by the user.

VII. Computational Aerospace and Biomechanical Applications

This section presents applications of NRM in aerospace and biomechanics. There are more research fields where NRM can be applied, for example, dynamics of mechanical systems with deformable-moving parts. The numerical Reuleaux method (NRM) is a geometricalcomputational algorithm to determine the instantaneous rotation center (IRC) for a deformable or pseudo-rigid body (PRB) in arbitrary movement. In recent International Scientific Contributions/Publications, the forward mathematical IRC problem (FP) was presented/determined for deformable solids, that is, given a defined arbitrary movement and random deformation, find the approximated IRC. We develop complementary simulations for this FP to corroborate its theoretical validation, and subsequently inverse methods are carried out. In other words, given an arbitrary rotation angle and a fixed IRC, find the optimal PRB deformation.

Furthermore, given a desired IRC, determine both the optimal rotation angle and deformation parameters for a movement. Analytic and numerical methods are carried out for these objectives with designed software both in Freemat and Matlab usually. Checking the results was carried out with FORTRAN 77 and 90 in many cases.
The principal algorithm for the mathematical model, was set as both forward and inverse problem optimization as,

$$f(\vec{x}) = \sum_{i=1}^{n} \frac{\int_{V_i} \rho_i(\vec{x_i}) dv}{\sum_{j=1}^{n} \int_{V_j} \rho_j(\vec{x_j}) dv_j} \times \left\| \vec{x} - \vec{x_i} \right\|^2$$

[Eq 80]

From this nonlinear optimization model, it is possible to select a desired IRC at any movement in function of the deformation and initial and final position, exclusively for a determined deformation, or combination of these physical conditions. In the following Figure 1, an aerospace illustrated example with an helicopter movement, provided the helicopter can change at flight its volume and gravity center, is presented. In Figure 7.1, it is explained for easy understanding a simple application.

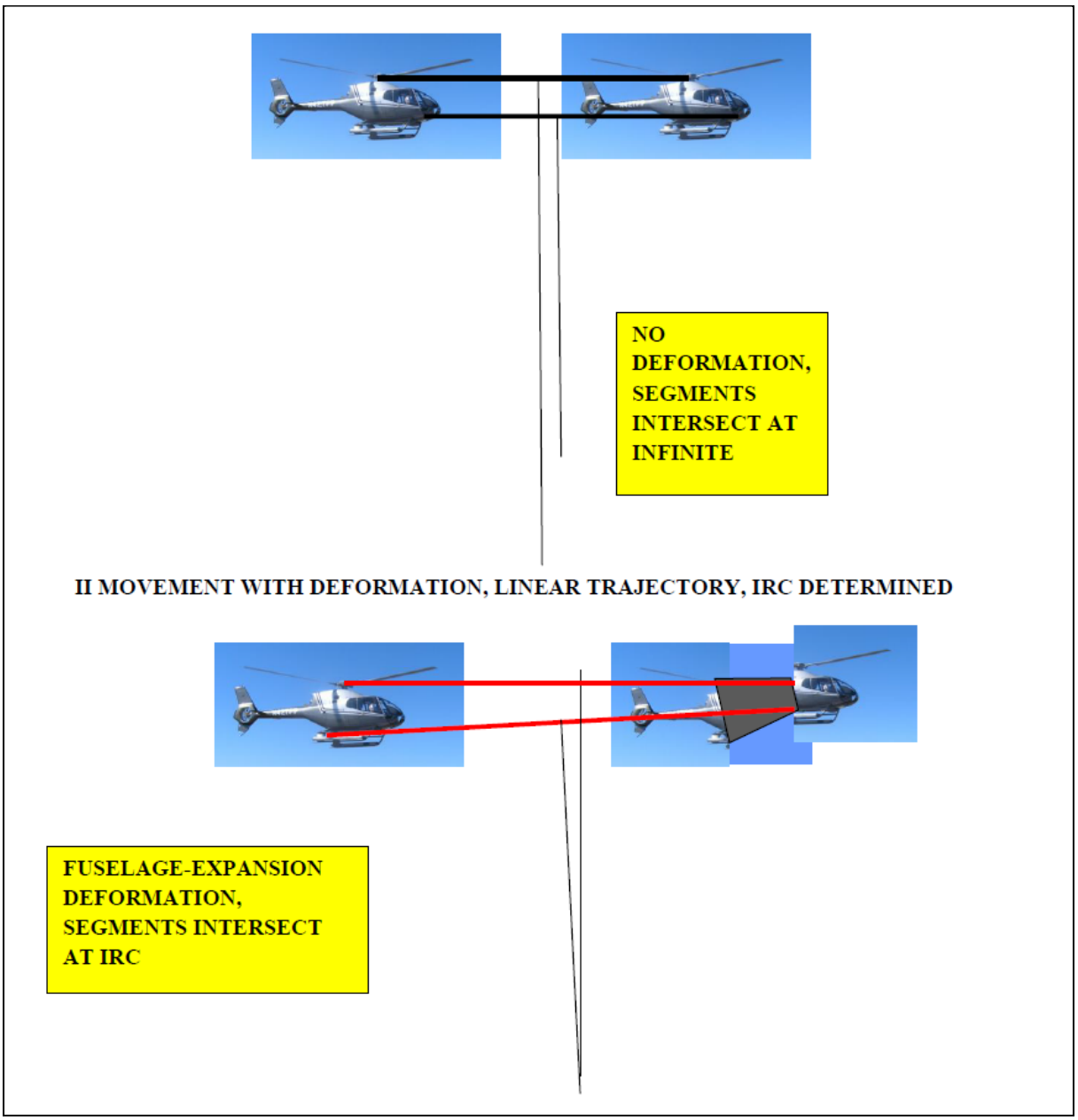

Figure 7.1.-Concept of NRM Mathematical Model application for aerospace fuselage changes.

The biomechanical application that is presented here refers to the movement of a spine artificial intervertebral disk. In Figure 7.2, it is shown how the voxelization can be done to determine the IRC when the spinal column moves, forward, backwards, lateral, oblique, etc. In Figure 7.3, a real radiological simulation is presented. The simulation gives an approximation of the IRC and was carried out in a water tank (tissue radiation-attenuation) with depth similar to the human body depth of spinal column within human body

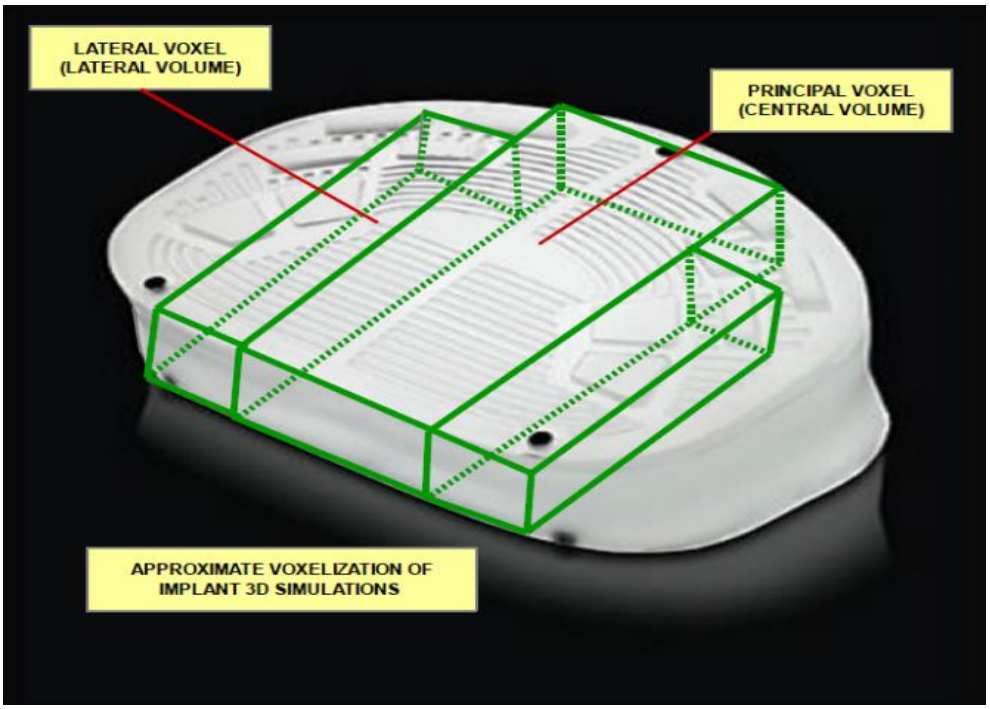

Fig 7.2.-Approximations for voxelization of the artificial lumbar disk to set the 3D simulations numerically for inverse determination of IRC (3D). The complete volume of the disk is almost covered, so the 3D simulation data could be approximated to the whole disk dynamics. We set 3 voxels for the most part of this volume of the disk, and next contributions will share all the resting wings-volume with 5 voxels. Note that the dark points over the disk surface correspond to radiological markers (60% tantalum composition after experimental optimization, that can be used during/after surgery to obtain an optimal setting of the disk. Sub-optimal position of the disk after operation could yield to paresthesias, severe radicular/disk pain, mobility difficulties, and in the long term increase of the biased position of the disk. This simulation was done by Casesnoves in Biomechanics Laboratory of Nottingham University in 2007.

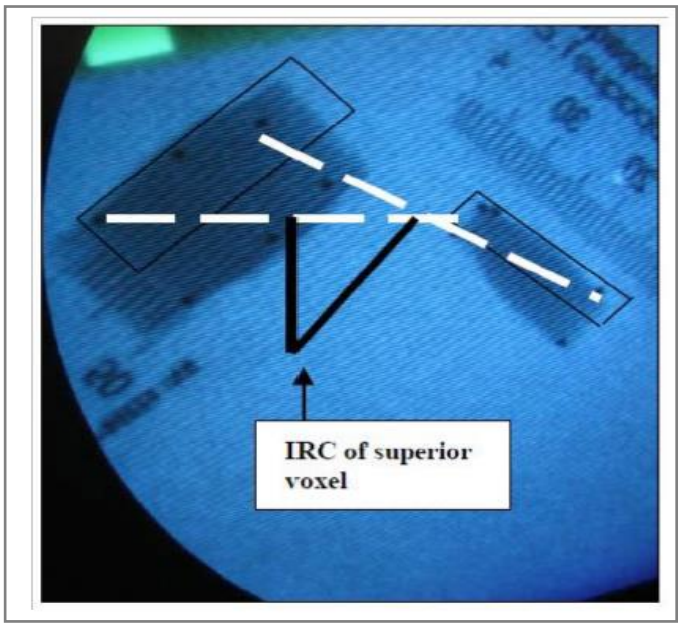

Fig 7.3.-Radiological Simulation for IRC approximate Determination with Implant Deformation.

A compliant artificial disk manufactured with composites and its radiological simulation for an exaggerated lumbar spine flexion-compression.These markers (Mixed Tantalum 60% from ref 7, principal) can be used for imaging position determination [ref 7]. We used, as said, for the realistic radiological screen-photography of this simulation a Siemens Siremobil 4K, C-Arm RX-Machine properly manufactured for surgical theatre. Distances are measured with a radiological rule that appears in image.This type of radiological apparatus are used in surgery to fit exactly the position of the artificial implant. The mechanical reason is that the arm of the machine can be moved along several angles/distances, in such a way that avoiding surgical sterilized blanketts and covers, or any anatomical part of the patient which is hindering the imaging-geometrical setting for good visualization at screen. In addition, in spinal surgery, and specially in lumbar disk pathology, it is not unfrequent to find obese patients who create radiological difficulties that can be overcome by the mechanical adaptation of this C-Arm machine. It was proven mathematically/simulations [Casesnoves,4,5,6,7],that the IRC/IAR of this implant can be approximated with these radiological imaging techniques using the Numerical Reuleaux Method. Furthermore, the precision of this IRC/IAR determination could be improved by using better imaging-radiological equipment, MRI or CT techniques, or standard radiological simulators [designed by Casesnoves,2008,proceedings of SIAM Conference in Computational Science/Engineering, 2009].

VIII. Discussion, Conclusions, and Applications

The Theoretical frame of the **NRM** has been conveniently proven through the most important laws of the Optimization Theory. The Convexity, Existence of a Global Minimum in **2D** and in **3D** (when the movement is pure in **3D)** has been mathematically demonstrated. Other Nonlinear properties of the Objective Funtion(s) have also been proven. We can assert that the Theory of the **NRM** is according to the current criteria about the feasibility to get a suitable Large-Scale Optimization process. The Simulations can be considered valid to go ahead towards a contundent and/or definite confirmation of the Model in experimental dynamics. This fact was confirmed in the subsequent publications from 2007The last stage would be an Experimental series of Laboratory work to mesh definitely the link between the theory and the practice.

The Simulations results show a clear Statistical advantage for the model when a large number of voxels is selected. In **2D**, the Average Error difference, in favour of the 2 voxels frame, is **≈ 6%** , and in the **3D** simulations it raises to **≈ 10%**. We cannot assert definitely the veracity of the Theory until a large number of further simulations will be carried out in future publications. These simulations would involve a random selection of rotation angles, initial position in the **2D** or **3D** space, and carry out the trials with different geometrical shapes. The applications of the Model could be focused on Engineering Mechanics and Industrial Machinery, Bioengineering, or Biomechanics [**11**], among several others.

The mathematical background of the **NRM** has been properly set at initial stages. Further improvements and better Objective Functions could be designed in new research. The results of the Primary Simulations show a difference of error in favour of the higher voxels number frame(s). However, longer and better Statistical trials will be convenient and necessary. The Future research is focused on Mechanical Engineering and Machinery, to apply the **NRM** directly on technical practice. The fields of Bioengineering, Biomechanics [**1.1**,**10**,**11**,**12**,**27**] , and Medical Devices Design [**11**], also constitute important application fields.

IX. REFERENCES

References 1st Group

[1]. Arnold, VI. Mathematical Methods of Classical Mechanics. 2nd Edition. Springer. 1989.

[2]. Bartholomew-Biggs, M. Nonlinear Optimization with Engineering Applications. Springer Optimization and its Applications. 2008.

[3]. Bazaraa, MS. Nonlinear Programming: Theory and Algorithms. 3rd Edition. Wiley-Interscience. 2006.

[4]. Bertsekas, DP. Nonlinear Programming. Second Edition. Athena Scientific. 2003.

[5]. Björck, A. Numerical Methods for Least Squares Problems. SIAM. 1996.

[6]. [5.1] Bonnans, JF, and Others. Numerical Optimization, Theoretical and Practical Aspects. Springer Universitext. 1997. [5.2] Borwein, JM, Lewis, AS. Convex analysis and nonlinear optimization: theory and examples. Springer. 2006.

[7]. Braess, D. Nonlinear Approximation Theory. Springer Series in Computational Mathematics. 1986.

[8]. Braess, D, Schumaker, LL. Numerical Methods in Approximation Theory. Vol 9. Birkhäuser International Series of Numerical Mathematics. 1992.

[9]. Bronstein, AM, Bronstein, MM, Kimmel, R. Numerical Geometry of Non-Rigid Shapes. Springer. 2008.

[10]. Buseman, H, Kelly, PJ. Projective Geometry and Projective Metrics. Dover Publications, Inc. 2006.

[11]. Casesnoves, F. 'A Monte-Carlo Optimization Method for the Movement Analysis of Pseudo-rigid Bodies'. 10th SIAM Conference in Geometric Design and Computing, Texas, San Antonio, USA. Contributed Lecture. November 2007.

[12]. Casesnoves, F. 'Experimental Simulations of the Numerical Reuleaux Method for Lumbar Artificial Disc Implants IRC Determination'. Oral Presentation-Poster. 2009 SIAM Conference in Computational Science and Engineering. Miami USA. March 2009.

[13]. Casesnoves, F. 'Optimal Nonlinear Approximations and Errors Reduction for Numerical Reuleaux Method (NRM) Simulations in Pseudo-Rigid Bodies Dynamics'. Lecture. (Nonlinear Approximation Group). 13th International Conference in Approximation Theory. San Antonio (TX) USA. March 2010.

[14]. Chapra, SC, Canale, RP. Numerical Methods for Engineers. Fifth Edition. McGraw-Hill. 2006.

[15]. Cheney, W, Light, W. A Course in Approximation Theory. American Mathematical Society. Series Graduate Studies in Mathematics. Vol. 101. 2000.

[16]. [15.1] Clark, William M, and Virginia Downward. Mechanical Models: A Series of Working Models on the Art and Science of Mechanics. Newark, NJ: Newark Museum, 1930.

[17]. [15.2] Cohen, H, Muncaster, RG. The Theory of Pseudo-Rigid Bodies. Springer-Verlag. New York. 1988.

[18]. Di Pillo, G, and Others. Large-Scale Nonlinear Optimization. Springer Series in Nonconvex Optimization and its Applications. Vol 83. 2006.

[19]. Edwards, J R. Advanced Calculus in Several Variables. Dover (Reprinted and Revised). 1994.

[20]. Friedman, A. Advanced Calculus. Dover (Reprinted and Corrected). 1999.

[21]. Fausett, LV. Applied Numerical Analysis

using Matlab. Second Edition. Pearson. 2008.

[22]. Higham, DJ, Higham, NJ. Matlab Guide. Second Edition. SIAM. 2005.

[23]. Hildebrand, FB. Introduction to Numerical Analysis. Second Edition. Dover Publications, Inc. 1987.

[24]. Jennings, GA. Modern Geometry with Applications. Springer. 1994.

[25]. Kaltenbacher, B, Neubaer, A, Scherzer, O. Iterative Regularization Methods for Nonlinear Ill-posed Problems. Radon Series on Computational and Applied Mathematics. De Gruyter. 2008.

[26]. Kariya, T, Hiroshi, K. Generalized Least Squares. Wiley Series in Probability and Statistics. 2004.

[27]. Kennedy, Alex B.W. Kinematics of Machinery, Two lectures relating to Reuleaux methods, delivered at South Kensington Museum. New York: D. Van Nostrand, 1881.

[28]. Kirsch, A. An Introduction to the Mathematical Theory of Inverse Problems. Springer. Applied Mathematical Sciences. Volume 120. 1996.

[29]. Komzsik, L. Approximation Techniques for Engineers. CRC Press. 2007.

[30]. Lewis-Beck, M. Applied Regression, An Introduction. Sage University Paper. C22. 1980.

[31]. Linchen, W. Data and Error Analysis. Prentice Hall. 1999.

[32]. Lipschutz, S, Lipson, M. Linear Algebra. 3rd Edition. Schaum's Outlines. McGraw-Hill. 2000.

[33]. Liu, SL. Monte-Carlo Strategies in Scientific Computing. Springer Series in Statistics. 2008.

[34]. Luenberger, DG. Linear and Nonlinear Programming. 2nd Edition. Corrected and Reprinted. Springer. 1972.

[35]. Miettinen, K. Nonlinear Multiobjective Optimization. Kluwer International Series in Operations Research & Management Science. Springer. 1998.

[36]. Nist-Sematech. E-Handbook of Statistical Methods. http//www.itl.nist.gov. div898/handbook/date,.

[37]. Pampel, F. Logistic Regression, A Primer. Sage University Paper (132). 2000.

[38]. Ralston, A, Rabinowitthz. A First Course in Numerical Analysis. Second Edition. Dover Publications, Inc. 2001.

[39]. Rankine, W. Manual of Machinery and Millwork. Vols.1,2. London: Griffin, 1887.

[40]. Reuleaux, F. Kinematics of Machinery. McMillan and Co., London. 1876.

[41]. Reuleaux, F. Lehrbuch der Kinematik, Vol. 1: Theoretische Kinematik. Braunschweig: F. Vieweg und sohn, 1875.

[42]. Rivlin, TJ. An Introduction to the Approximations of Functions. Dover Publications, Inc. 1969.

[43]. Sawaragi, Y, and Others. Theory of Multiobjective Optimization. Academic Press. Mathematics in Science and Engineering Series. Vol 176. 1985.

[44]. Schröder,J. Catalog of Reuleaux Models: Polytechnisches Arbeits-Institut. Illustrationen von Unterrichts-Modellen und Apparateni. Publisher Darmstadt: Polytechnisches Arbeits-Institut, 1899.

[45]. Smith, DM. Engineering Computation with Matlab. Pearson. 2008.

[46]. Venkataraman, P. Applied Optimization with Matlab Programming. Theoretical and Practical Aspects. 2nd Edition. Wiley Interscience. 2002.

[47]. Wolberg, J. Data Analysis Using the Method of Least Squares. Springer. 2006.

[48]. Wrede, RC, Spiegel, M. Advanced Calculus. Second Edition. Schaum's Outlines. McGraw-Hill. 2002.

References 2nd Group

[1]. Casesnoves F, Suzenkov A. Mathematical Models in Biotribology with 2D-3D Erosion Integral-Differential Model and Computational-Optimization/Simulation Programming. International Journal of Scientific Research in Computer Science, Engineering and Information Technology. 2017 IJSRCSEIT | Volume 2 | Issue 3 | ISSN : 2456-3307.

[2]. Casesnoves F, Antonov M, Kulu P. Mathematical models for erosion and corrosion in power plants. A review of applicable modelling optimization techniques. IEEE Xplore database and will be cross referred in SCOPUS. Proceedings of RUTCON2016 Power Engineering Conference.2016Riga Technical University.

[3]. Casesnoves, F. 2D computational-numerical hardness comparison between Fe-based hardfaces with WC-Co reinforcements for Integral-Differential modelling. Key Engineering Materials Journal. Trans Tech publications 2018. Vol 762, pp 330-338. DOI: 10.4028/www.scientific.net/KEM.762.330.ISSN: 1662-9795. 2018.

[4]. Casesnoves F, Surzhenkov A. Inverse methods for computational simulations and optimization of erosion models in power plants. IEEE Proceedings of RUTCON2017 Power Engineering Conference.Riga Technical University. IEEExplore Publication in 5th December 2017. DOI:10.1109/RTUCON.2017.8125630. Electronic ISBN:978-1-5386-3846-0. USB ISBN: 978-1-5386-3844-6.Print on Demand (PoD) ISBN: 978-1-5386-3847-7.

[5]. Kulu P, Casesnoves F, Simson T, Tarbe R. Prediction of abrasive impact wear of composite hardfacings. Solid State Phenomena, Proceedings of 26th International Baltic Conference on Materials Engineering. 2017. Solid State Phenomena Submitted: 2017-06-12. ISSN: 1662-9779, Vol. 267, pp 201-206. DOI:10.4028/www.scientific.net/SSP.267.201 2017 Trans Tech Publications, Switzerland Online: 2017-10-10.

[6]. Surzhenkov A, Viljus M, Simson T, Tarbe R, Saarna M, Casesnoves F. Wear resistance and mechanisms of composite hardfacings atabrasive impact erosion wear. IOP Conf. Series: Journal of Physics: Conf. Series 843 (2017) 012060 doi :10.1088/1742-6596/843/1/012060.

[7]. P. Kulu, R. Tarbe, A. Zikin, H. Sarjas, A. Surženkov, Abrasive wear resistance of recycled hardmetal reinforced thick coating, Key Eng. Mat. 527 (2013) 185-190.

[8]. A. Surzhenkov, R. Tarbe, M. Tarraste, T. Simson, M. Viljus, P. Kulu, Optimization of hardmetal reinforcement content in Fe-based hardfacings for abrasive-impact wear conditions, Proc. Eur. Conf. Heat Treat. 2016 and 3rd Int. Conf. Heat Treat. Surf. Eng. Automotive Applications, 11–13 May 2016, Prague, Czech Republic.

[9]. Antonov,M, Renno Veinthal Elina Huttunen-Saarivirta Irina Hussainova, Ahto Vallikivi, MartynasLelis, Jelena Priss. 'Effect of oxidation on erosive wear behaviour of boiler steels'. Tribology International 68 (2013) 35–44.

[10]. Kleis, I, Kulu, P. Solid Particle Erosion. Springer. 2008.

[11]. Shin J, Jeon Y, Maeng,. Kim,J. Ro. Analysis of the dynamic characteristics of a combined-cycle power plant. Energy 27 (2002) 1085–1098.

[12]. Casesnoves, F. 'Computational Simulations of Vertebral Body for Optimal Instrumentation Design'. ASME Journal of Medical Devices (Research Paper). Author: F Casesnoves .Journal of Medical Devices. June 2012.

Volume 6. Issue 2/021014.11 pages.http://dx.doi.org/10.1115/1.4006670.

[13]. Chen Q, Li D. Computer simulation of solid-particle erosion of composite materials. Wear 255 (2003) 78–84.

[14]. Antonov, M. Assessment of Cermets Performance in Aggressive Media. Doctoral Dissertation, thesis. thesis on mechanical and instrumental engineering 29.TUT Press. 2006.

[15]. Abramobitz, Stegun. Handbook of Mathematical Functions. Applied Mathematics Series. 55.1972.

[16]. Crocker, L. A review of current methods for modeling erosive wear. NPL Report. 2011.

[17]. Li L, Li D. Simulation of corrosion-erosion of passive metals using a micro-scale dynamical model. Wear 271 (2011) 1404– 1410.

[18]. Tribocorrosion:research, testing, and applications. Selected Technical Papers. International Standards Worldwide. ASTM, STP#1563.

[19]. Todinov, M. Reliability and Risk Models. Wiley. 2005.

[20]. Luenberger, G D. Linear and Nonlinear Programming. Fourth Edition.Springer.2008.

[21]. Casesnoves,F.'Large-Scale Matlab Optimization Toolbox (MOT) Computing Methods in Radiotherapy Inverse reatment Planning'. High Performance Computing Meeting. Nottingham University. January 2007.

[22]. Casesnoves, F. 'A Monte-Carlo Optimization method for the movement analysis of pseudo-rigid bodies'. 10th SIAM Conference in Geometric Design and Computing, Texas, San Antonio, USA. Contributed Talk. November 2007.

[23]. Derrick O. Njobuenwu, Michael Fairweather. Modelling of pipe bend erosion by dilute particle suspensions. Computers and Chemical Engineering 42 (2012) 235– 247.

[24]. Casesnoves, F. 'Applied Inverse Methods for Deformable Solid Dynamics/Kinematics in Numerical Reuleaux Method (NRM)'. International Journal of Numerical Methods and Applications. volume 9(2) 2013 .pages 109-131. peer-reviewed International Mathematical/Computation Journal Article. print/Online.http://www.pphmj.com/abstract/7688.htm. This article is specially innovative in Inverse Problems applications for deformable solids kinematics/dynamics, further publications are included in United States Congress Library and Numerical Reuleaux Method is accepted by scientific community as an innovative dynamics method in deformable solids with mechanical, biomechanical and aerospace applications. New applications of this method will be probably found significantly in future.

[25]. Mayusama, F.'History of Power Plants and Progress in Heat Resistant Steels'. International Journal of the Iron and Steel Institute of Japan ISIJ International, Vol. 41 (2001), No. 6, pp. 612–625.

[26]. Woytowitz ,P, Richman R. Modeling of damage from multiple impacts by spherical particles. Wear 233–235 .999. 120–133.

[27]. Li D, Elalem K, Anderson M, Chiovelli S. A microscale dynamical model for wear simulation. Wear 225–229 .1999. 380–386.

[28]. Matthews A, Franklin S, and Holmberg K. Tribological coatings: contact mechanisms and selection. J. Phys. D: Appl. Phys. 40 (2007) 5463–5475.

[29]. Liao H, Normand B, Coddet C. Influence of coating microstructure on the abrasive wear resistance of WC/Co cermet coatings. Surface and Coatings Technology 124 (2000) 235–242.

[30]. 'European Textbook on Ethics in Research'. European Commission, Directorate-General for Research. Unit L3. Governance and Ethics. European Research Area. Science and Society. EUR 24452 EN.

[31]. Casesnoves, Antonov, Kulu. Mathematical Models for Erosion and Corrosion in Power

Plants. A Review of Applicable Modelling Optimization Techniques. 2016// 57th International Scientific Conference on Power and Electrical Engineering of Riga Technical University (RTUCON). 2016.

[32]. Casesnoves, F. Applied Inverse Methods for Optimal Geometrical-Mechanical Deformation of Lumbar artificial Disks/Implants with Numerical Reuleaux Method. 2D Comparative Simulations and Formulation. Computer Science Applications. Volume 2, Number 4, pp. 1-10. www.ethanpublishing.com. This article is registered as original method published by Francisco Casesnoves in Philadelphia 2015 in United States Congress Library.

[33]. Notes, References, and Lectures of CEE SIMP Conference. Raw Materials and Circular Economy. Institute of Geology, Tallinn University of Technology. Mektori Technology Innovation Center. June 2017.

[34]. Tanning, Lembo. Maailma Energia Ulevaade. III Osa. Alternaatiivised susi hudro tulevik. Tallinn 2010. Marcelus Trade OU.

[35]. Tanning, Lembo. Maailma Energia Ulevaade. II Osa. Tuumaenergia. Tallinn 2010. Marcelus Trade OU.

[36]. Tanning, Lembo. Maailma Energia Ulevaade. I Osa. Nafta, Gaas. Tallinn 2010. Marcelus Trade OU.

[37]. Holmberg K, Erdemir A. Influence of Tribology on Global Energy Consumption, Costs, and Emissions. Friction 5(3):263-284.2017.

[38]. European Textbook on Ethics in Research. European Commission, Directorate-General for Research. Unit L3. Governance and Ethics. European Research Area. Science and Society. EUR 24452 EN.

[39]. Casesnoves, F. Nonlinear comparative optimization for biomaterials wear in artificial implants technology. Presented in Applied Chemistry and Materials Science RTU2018 Conference Proceedings. 2018.

Author's Biography

Francisco Casesnoves is Engineering PhD by Talllinn University of Technology (started thesis in 2016, thesis defence/PhD-graduated in 2018), Estonia, and computational-engineering/physics independent researcher at COE, MSc-BSc, Physics/Applied-Mathematics (Public Eastern-Finland-University), Graduate-with-MPhil, in Medicine and Surgery (Public Madrid University Medicine School). Casesnoves studied always in public-educational institutions. His education/scientific vocation was motivated very young, by Profs Candida Navamuel and Isabel Vela, in Renaissance-Humanism ideas—later on with the motivation manuscripts of Nobel and Von Helmholtz prizes Santiago Ramon y Cajal. His constant service to International Scientific Community and Estonian technological progress (2016-present) commenced in 1985 with publications in Medical Physics, with further specialization in optimization methods in 1997 at Finland—at the moment approximately 90 recognized publications. As physician, he worked in medical practice while medical student at Madrid Clinical Hospital and Madrid Central Defence Hospital. His main branch is Computational-mathematical Nonlinear/Inverse Optimization. His service to International Scientific community also comprises the publication of two recent books with Estonian affiliation, the first is the computational dynamics book, 'The Numerical Reuleaux Method' (200 pages, first part book, 2019), the second is a sociological and medical philosophy book (300 pages, 2019). Casesnoves best-achievement is the Numerical Reuleaux Method in dynamics and nonlinear-optimization. This Numerical Reuleaux Method constitutes, among others, an advance in Space Aerodynamics Computational Methods and Bioengineering. Casesnoves speaks, reads, and writes Estonian language at B1-2 levels, with corresponding official Innove Diplomas in A2 and B1. Also participates/registers in sporting Estonian activities such as Tallinn Marathon. Casesnoves played as defender and middle-fielder at Junior Madrid Football League, and as

physician is supporting agnostic healthy life and all sporting activities. His publications are always according to International Scientific Standards. He sets his medical technology papers, specially in cancer radiotherapy methods, always in open access for benefit and use of any public health system according to the Fundamental Right for health care. Recently has written new mathematical modelling radiotherapy articles affiliated to Estonia, Tallinn (2019). Casesnoves has contributed to technological development in Estonia (and also at Riga technical University, Power Electrical and Electronics Department) with 19 articles, two books, and 1 industrial project associated to Europa Union EIT Health Program (Tartu University, 2017). In EIT Europa Union Program, Tartu University, He developed his invention of the radiotherapy conformal wedge based on AAA radiotherapy model (Anisotropic Analytical Algorithm) with implemented Software-Engineering ja simulations in Matlab-Freemat, Fortran, and F#.

Appendix

Figures and Computational Tables

APPENDIX 1

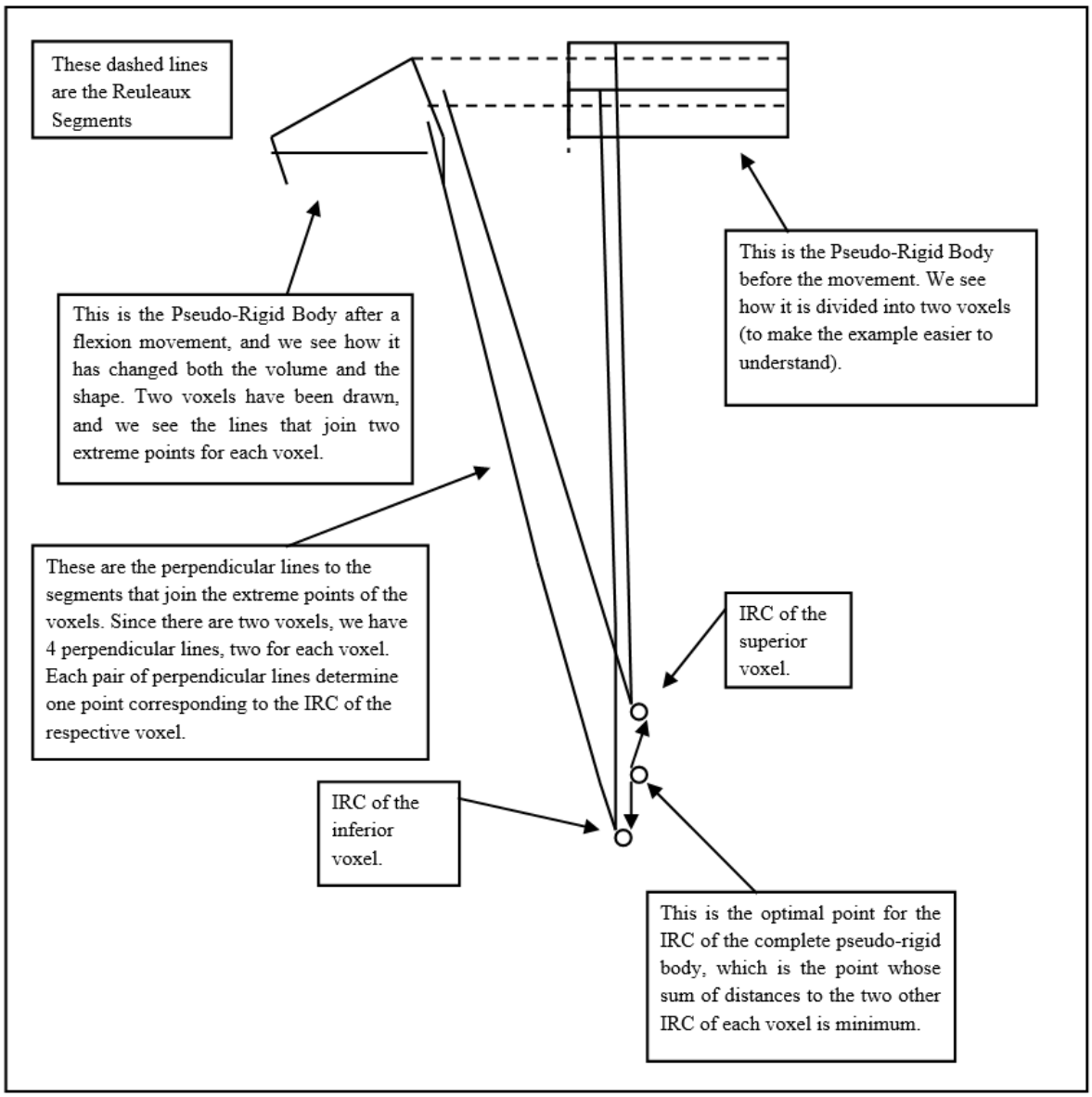

Fig 3 (Appendix 1).- A simple scheme of the idea of the Numerical Reuleaux Method with additional explanations. We can see how the changes of shape and volume are causing a variation on the IRC position. The optimal IRC is calculated by a **LSM** which obtains the best approximated point whose sum of distances to all the sparsed particular IRCs for each voxel is minimal.

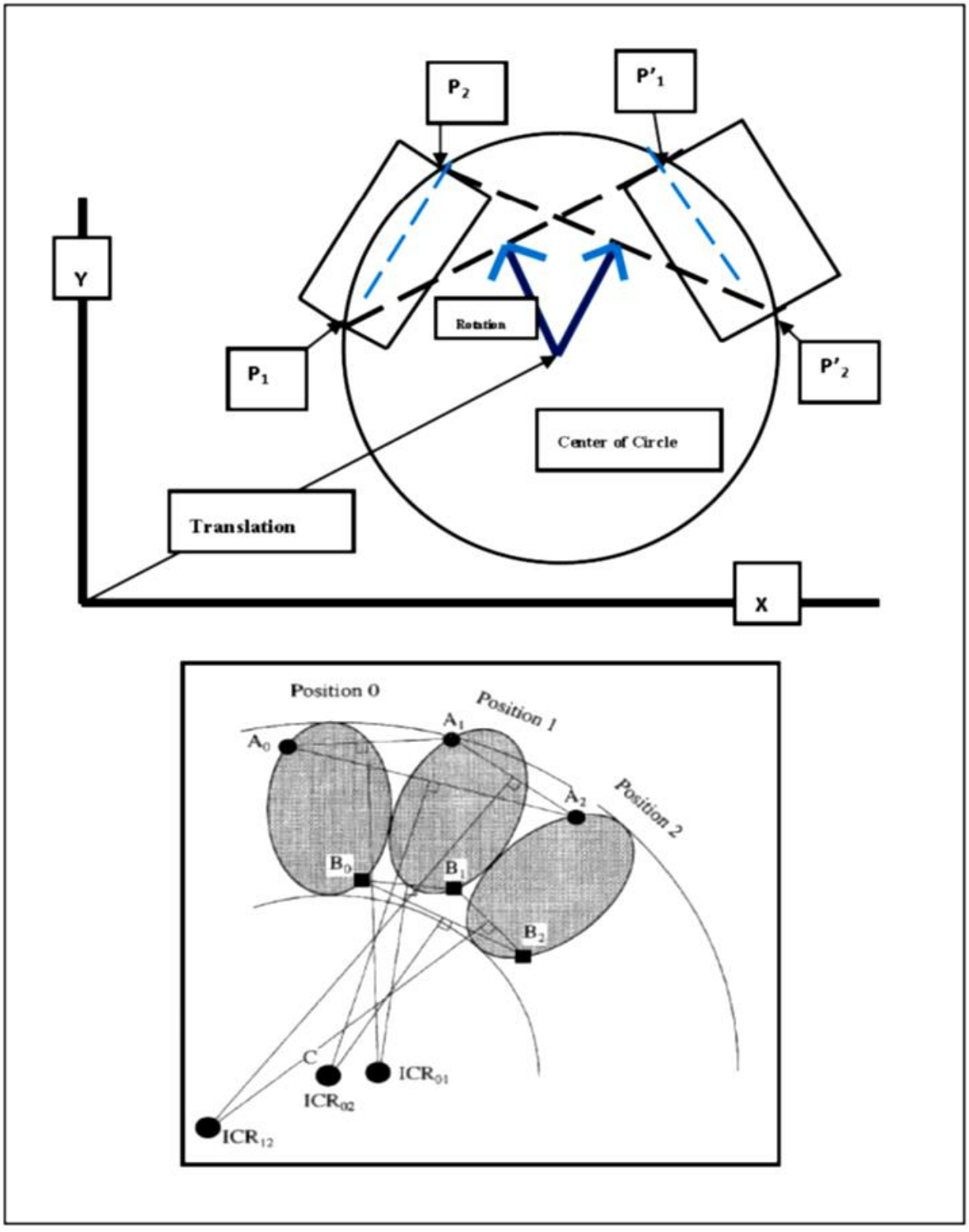

Fig 3 Complementary (1).-2D Geometric demonstration of the circle that is obtained when applying the RM for a rigid body. We see how the RM takes those fixed points of the Rigid Body, at initial and final positions, and then we draw the perpendicular to the middle points. The Reuleaux segments are the cords of the rotation circle, and the perpendiculars are radii of that circle. The lower Figure from a Biomechanics Paper (Chen, J, and Others. The limitations of the Instantaneous Centre of Rotation in joint research. Journal of Oral rehabilitation. 1999.) shows how the IRC is analyzed through a sequence of movements, and the variation of its position in **2D**. We show also clearly the movement decomposition in a translation respect to the coordinates origin, and a rotation respect to the IRC (Reuleaux Center). This is shown in the following **Figure 3C(2)**.

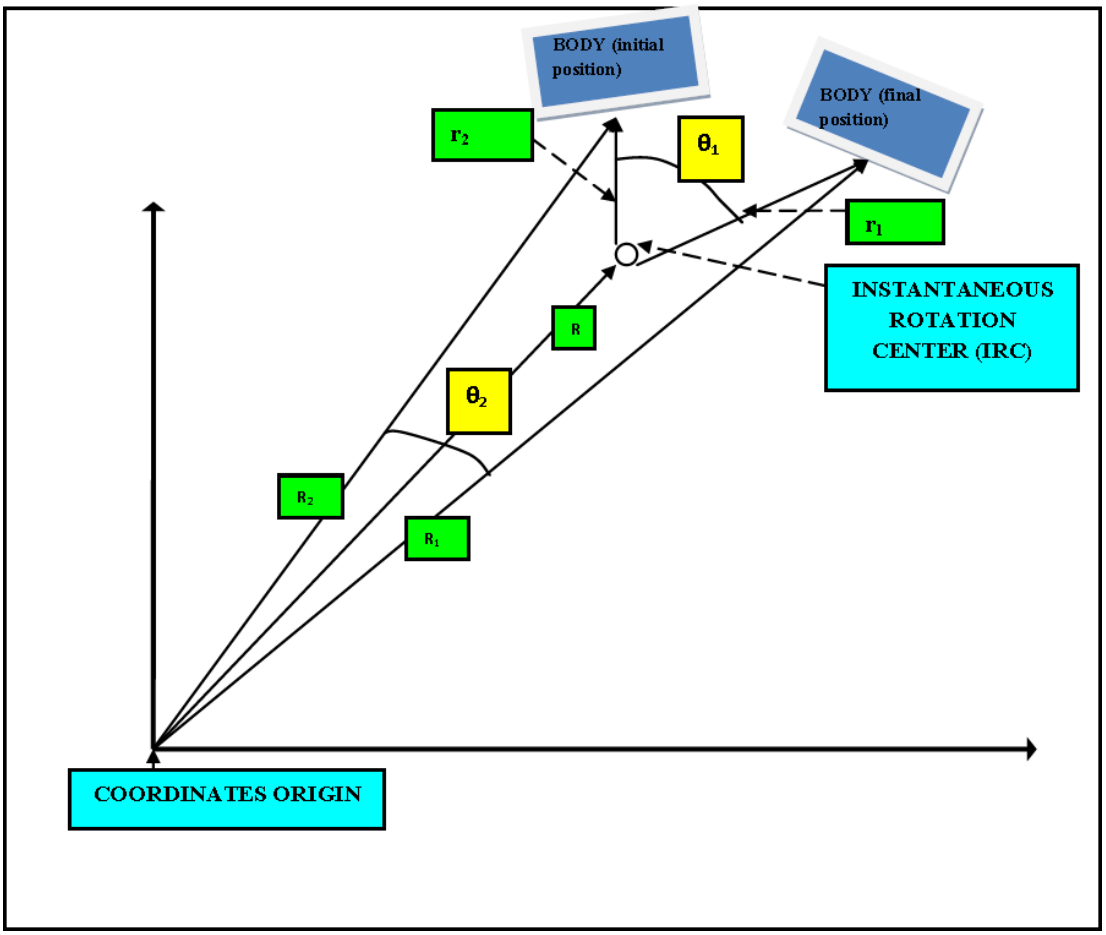

Fig 3C (2).-Here is the basic scheme of the translation that has to be done to calculate the distances and movement angles from the Coordinates Center to the Rigid Body Position. The Rotation angle around the Reuleaux IRC is θ_1. Vector Calculations are as follows

$\vec{R}, \vec{R}_1$ and $\vec{R}_2$. And $\vec{R}_1$ and $\vec{R}_2$ define the angle θ_2 through their dot product. $\vec{R}$ head point is given by the Reuleaux geometrical calculation, no matter where the coordinates origin is. Now, we get the following vectors

$\vec{r}_1=\vec{R}_1-\vec{R}$

$\vec{r}_2=\vec{R}_2-\vec{R}$, and both $\vec{r}_1$ and $\vec{r}_2$ define the angle θ_1 through their dot product.

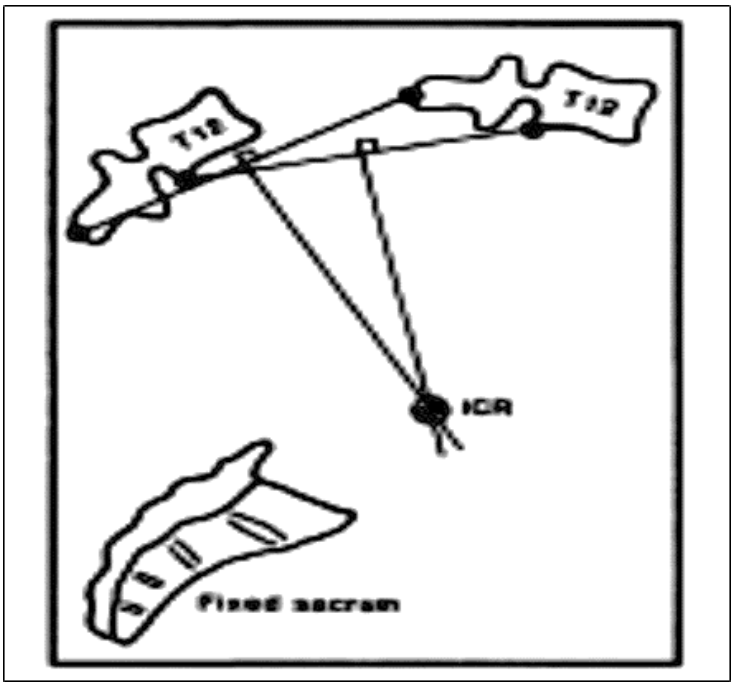

Fig 3C(3).-Here is an example of application of the Reuleaux Method for Rigid Bodies on Biomechanics. The sketch shows how the **2D** IRC of the vertebrae during a movement of extension is determined (in **2D** the IRC is not properly an 'IRC'. We get the Geometric place of an Axis of Rotation for any slide of the body that we get in **2D** (or any infinitesimal **2D** planar slide), not formally a point. However, if we have a Body that rotates in **2D**, and we get the Geometrical Space position, we can carry out reasonable approximations to select an optimal point of that Axis, that could be considered as the Approximated IRC for the entire Body). This Reuleaux **2D** method is extensively used in Spinal Biomechanics with important and practical Bioengineering applications. We see in the sketch how two points of the vertebrae are selected, and the Reuleaux segments are traced. The intersection of the middle points perpendiculars to these segments give the IRC in **2D**. These techniques are applied usually in Radiology and Magnetic Resonance to determine the IRC in Lumbar Spine Biomechanics Research. Measurements and calculations are also frequently made **in vitro** with anatomical specimens, and also with Spine Simulators. However, further physiological measurements advances could be developed through similar or new Imaging Techniques.

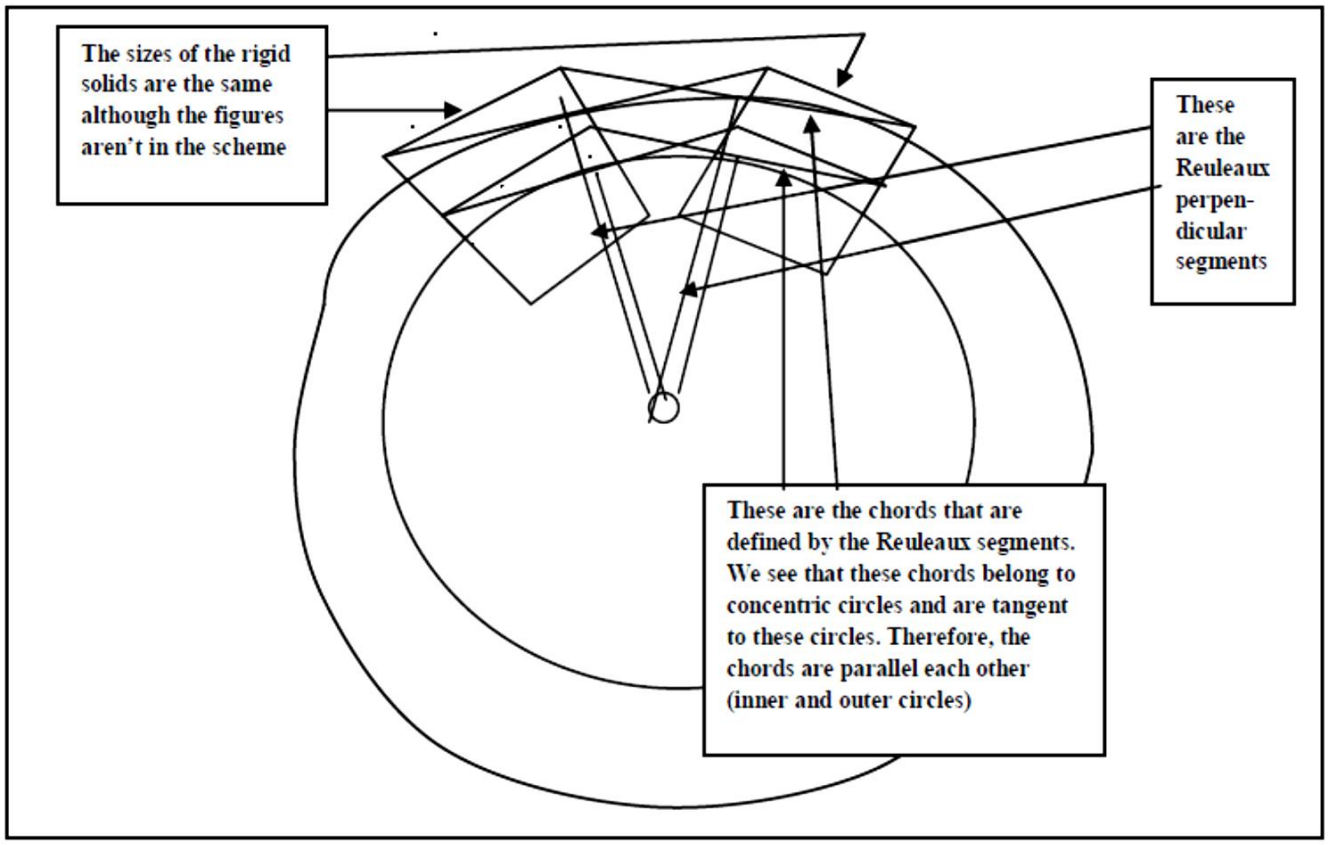

Fig 4.-Basic scheme of the initial assumption [**2.1**] with additional comments. The volume of the rigid body is the same despite the drawing errors, before and after the movement.

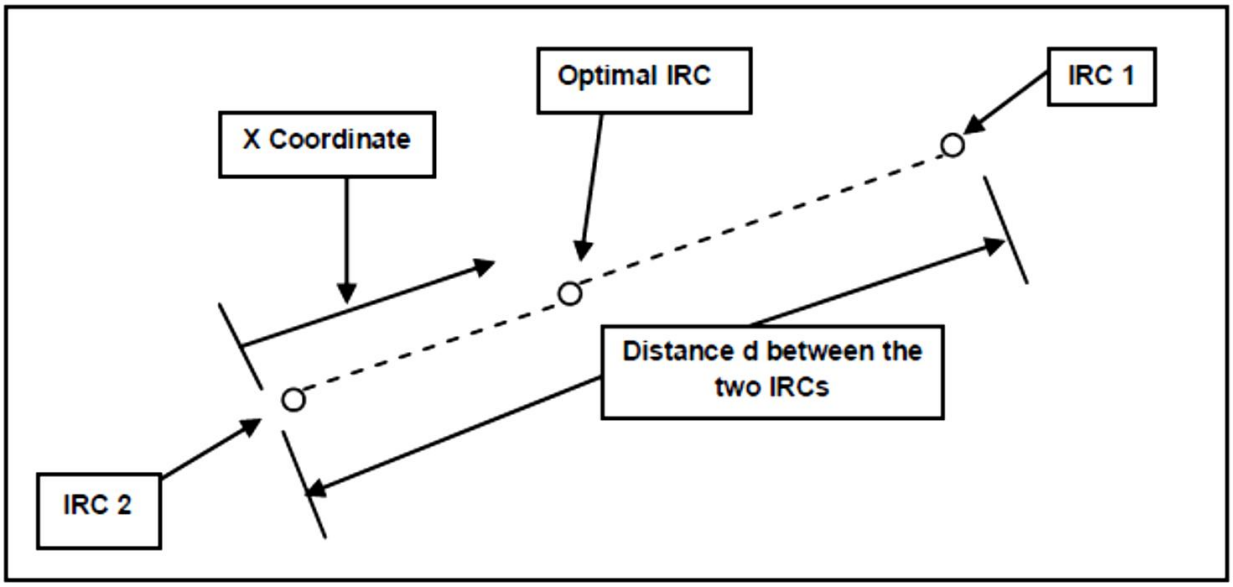

Fig 5.-Basic scheme of the simple model for two IRCs in a two-voxels division. This is a simplified sketch to make a concept caption easy.

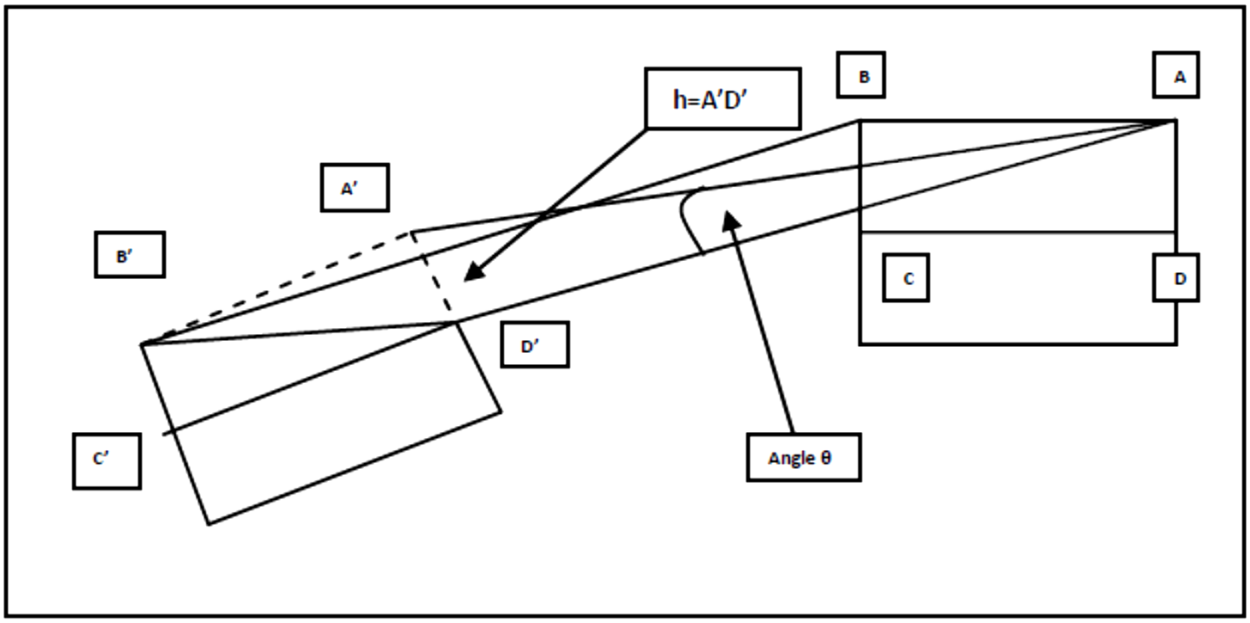

Fig 5.1.-The basic scheme for the demonstration of the **Theorem 1**.

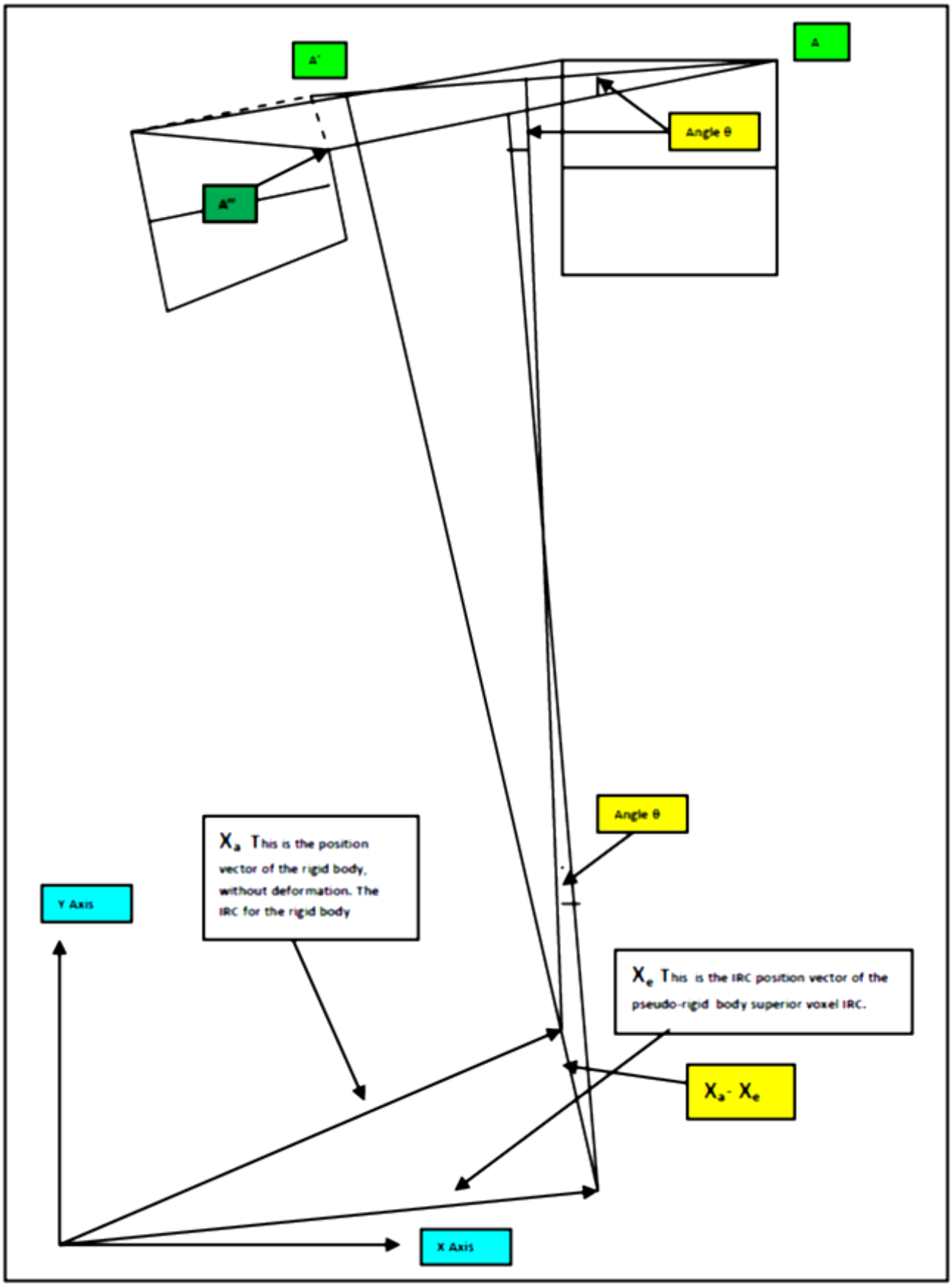

Fig 6.-Basic scheme for the demonstration of the **Theorem 3**.The distance **h**, **[Eq 56]**, is equal to A'A''.

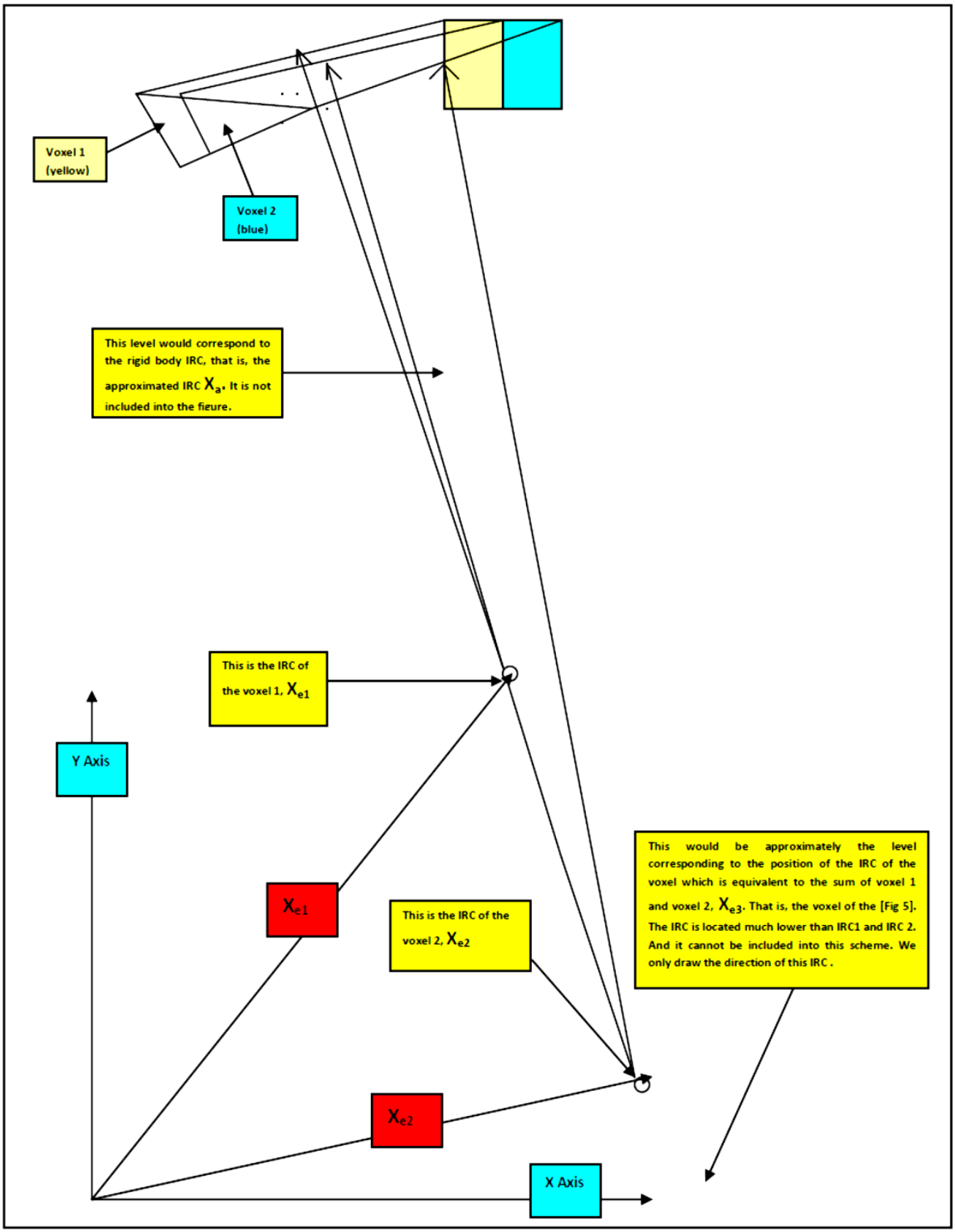

Fig 7.-This is the basic scheme to show the second part of **Theorem 3**. Some IRC points are not included into the figure because of their long distances.

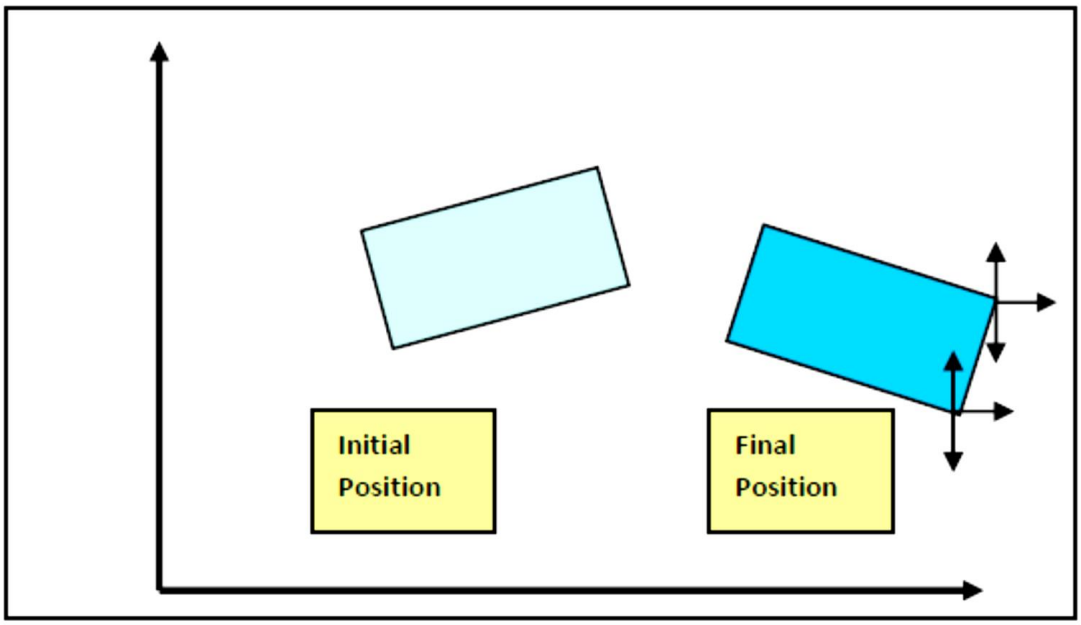

Fig 8.-Basic scheme of the random deformation of the final position that was carried out in the **2D** simulations. The deformations were both in X axis direction and Y axis direction.

2D SIMULATIONS FOR 1 VOXEL					
Simulation	Random Value of Deformation(s) (Approximated) and Coordinate(s) where they are applied on	RMS Error (Average for X and Y Coordinates*)	IRC Approximated for 1 Voxel	Optimized Rotation Matrix (Pseudo-Orthogonal)	Comments
1	Y +0.5 -0.5	0.2506	X=3.3820 Y=4.7512	A=-0.1121 B=-0.9932	_
2	Y +1 -0.5	0.1294	X=2.8750 Y=3.7500	A=0.2000 B=-0.9714	_
3	Y +0.25 -0.25	0.1411	X=3.6652 Y=4.8393	A=-0.1984 B=-0.9624	_
4	Y +0.25 -1	0.3534	X=3.8750 Y=4.8750	A=-0.1957 B=-0.8478	_
5	Y +0.35 -0.75	0.2571	X=3.6907 Y=4.7715	A=-0.1969 B=-0.9238	_
6	X= (rand (1)-0.5) Y= (rand (1)-0.5)	0.1323	X=3.6422 Y=5.0310	A=-0.2130 B=-0.9746	_
7	X= (rand (1)-0.5) Y= (rand (1)-0.5)	0.0243	X=3.6775 Y=4.7751	A=-0.0480 B=-0.9988	_
8	X= (rand (1)-0.5) Y= (rand (1)-0.5)	0.2385	X=3.5757 Y=5.0774	A=-0.3130 B=-0.9410	_

9	X= (rand (1)-0.5) Y= (rand (1)-0.5)	0.1316	X=3.4509 Y=3.5111	A=-0.3787 B=-0.9241	_
10	X= (rand (1)-0.5) Y= (rand (1)-0.5)	0.2876	X=3.5941 Y=5.1193	A=-0.3239 B=-0.9365	_
AVERAGE	N/A	0.1946	X=3.5428 Y=4.6501	N/A	_
Comments	The deformations do not exceed one unit in absolute value. Given the dimensions of the PRB, these values are rather high.	Error values about 20%. *See Error Calculations Formulas.		The elements of the pseudo-orthogonal matrix are almost null, which makes the matrix rather singular.	

Table 1.-These are the results for **2D** Simulations with one voxel. The average error is about 20%. The optimized elements of the Pseudo-Orthogonal matrix are shown. Note that this rotation matrix is defined after the translation of the approximated IRC to the Coordinates System Center.

2D SIMULATIONS FOR 2 VOXELS					
Simulation	Random Value of Deformation(s) (Approximated) and Coordinate(s) where they are applied on	RMS Error (Average for X and Y Coordinates*)	IRC Approximated for 2 Voxels	imized Rotation Matrix (Pseudo-Orthogonal)	Comments
1	Y +0.5 -0.5	0.1713	X=3.3800 Y=4.7500	A=-0.1121 B=-0.9932	_
2	Y +1 -0.5	0.0942	X=3.4661 Y=4.6232	A=0.2000 B=-0.9714	_
3	Y +0.25 -0.25	0.0668	X=3.5124 Y=4.4365	A=-0.1984 B=-0.9624	_
4	Y +0.25 -1	0.3793	X=5.5937 Y=4.1250	A=-0.1957 B=-0.8478	_
5	Y +0.35 -0.75	0.0746	X=3.5239 Y=4.3929	A=-0.1969 B=-0.9238	_
6	X=(rand (1)-0.5) Y=(rand (1)-0.5)	0.0975	X=3.5962 Y=4.5042	A=-0.2130 B=-0.9746	_
7	X=(rand (1)-0.5) Y=(rand (1)-0.5)	0.1321	X=3.4598 Y=4.6784	A=-0.0480 B=-0.9988	_

8	X=(rand (1)-0.5) Y=(rand (1)-0.5)	0.0949	X=3.5908 Y=4.5430	A=-0.3130 B=-0.9410	_
9	X=(rand (1)-0.5) Y=(rand (1)-0.5)	0.1138	X=3.4946 Y=4.6597	A=-0.3787 B=-0.9241	_
10	X=(rand (1)-0.5) Y=(rand (1)-0.5)	0.0744	X=3.4671 Y=4.3416	A=-0.3239 B=-0.9365	_
AVERAGE	N/A	0.1299	X=3.7085 Y=4.5055	N/A	_
Comments	In the second part of the simulations (6-10), we introduced more arbitrary variation of volume.	Lower figures compared to 1 Voxel 2D simulations (about 6%).			

Table 2.-Here we show results for 10 random simulations in **2D**, 2 voxels. Error value on average is about 13%.

2D SIMULATIONS FOR 2 VOXELS WITH LARGE DEFORMATION				
Simulation	Random Value of Deformation	RMS Error (Average for X and Y Coordinates*)	IRC Approximated for 2 Voxels	Optimized Rotation Matrix
1	X1=+0.5 X2=-0.5	0.1724	X=3.5734 Y=4.0949	A=0.1958 B=-0.9748
2	X1=+0.75 X2=-0.75	0.1822	X=3.4458 Y=4.5478	A=-0.1431 B=-1.0053
AVERAGE	N/A	0.1773	X=3.5096 Y=4.3214	N/A
Comments		Although the deformation is rather large, the Error values are about 18%. Note that there are only two random Simulations in this case. *See Error Calculations Formulas.		

Table 3.-This table shows the results for a reduced group of two random large-deformation **2D** simulations for 2 voxels. The resulting RMS error on average is about 18%.

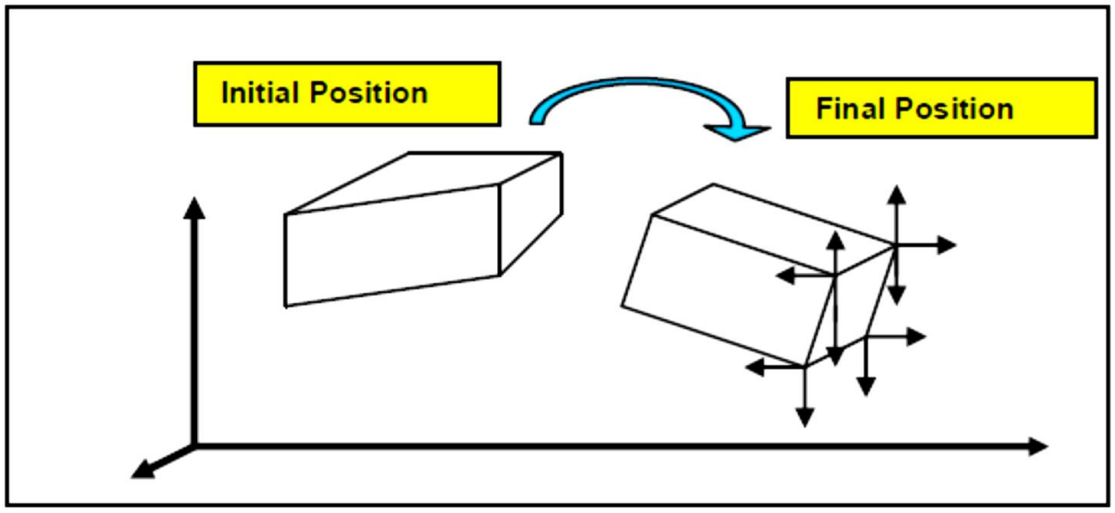

Fig 9.-Basic scheme of the random deformation of the final position that was carried out in the **3D** simulations.

3D SIMULATIONS FOR 1 VOXEL					
Simulation	Random Value of Deformation(s) (Approximated) and Coordinate(s) where they are applied on	RMS Error (Average for X,Y and Z Coordinates*)	IRC Approximated for 1 Voxel	Optimized Rotation Matrix (Pseudo-Orthogonal)	Optimization Residuals
1	Y=0.5 , -0.5 Z=-1 , -1	0.2172	X=3.8958 Y=4.2333 Z=4.8167	--------	—
2	Y=-1 , -0.2 Z=-1 , -1	0.1862	X=3.3367 Y=4.6848 Z=3.0315	A(1)=-0.0725 A(4)=-1.1730 A(7)=0.2084 A(2)=1.1427 A(5)=-0.3561 A(8)=-0.4101 A(3)= 0.0166 A(6)=-0.0332 A(9)=0.9522	—
3	Y=0.25 , -0.25 Z=-1 , -1	0.1596	X=3.6504 Y=4.4048 Z=4.0280	A(1)=0.0481 A(4)=-1.0233 A(7)=0.1930 A(2)=0.9072 A(5)=-0.0711 A(8)=-0.3723 A(3)=-0.0035 A(6)=0.0238 A(9)=0.9859	—
4	Y=-0.5 , -0.5 Z=-1 , -1	0.2939	X=4.3438 Y=3.9375 Z=6.3125	A(1)=0.2172 A(4)=-1.1517 A(7)=0.1544 A(2)=0.6178 A(5)=-0.2379 A(8)=-0.2718 A(3)=0.0286 A(6)=0.1552 A(9)=1.0203	ResNorm(1)=0.5213 ResNorm(2)=1.1059 ResNorm(3)=0.2636

5	Y=-0.2 , -0.2 Z=-1 , -1	0.2365	X=3.7608 Y=4.3394 Z=4.4112	A(1)=0.0813 A(4)=-1.1353 A(7)=0.1897 A(2)=0.8472 A(5)=-0.2799 A(8)=-0.3564 A(3)=-0.0022 A(6)=0.0634 A(9)=0.9949	ResNorm(1)=0.0788 ResNorm(2)=1.0020 ResNorm(3)=0.4292
6	X=0.4134 Y=0.1324 Z=-0.4025	0.5987	X=7.7715 Y=4.7658 Z=4.7216	A(1)=0.5283 A(4)=-0.5297 A(7)=0.5741 A(2)=0.5339 A(5)=-0.8028 A(8)=-0.5066 A(3)=0.1193 A(6)=0.2633 A(9)=0.6296	ResNorm(1)=1.4699 ResNorm(2)=2.1709 ResNorm(3)=1.7316
7	X=0.5202 Y=0.2746	0.0699	X=3.4493 Y=4.1399 Z=3.0385	A(1)=0.1606 A(4)=-1.0005 A(7)=0.3285 A(2)=0.9384 A(5)=0.2185 A(8)=-0.2128 A(3)=-0.0107 A(6)=0.0642 A(9)=0.9654	ResNorm(1)=0.3505 ResNorm(2)=1.8242 ResNorm(3)=3.5055
8	X=0.4966 Y=0.5283 Z=0.2760	0.1363	X=-0.1468 Y=-0.5177 Z=-8.8113	A(1)=-0.0681 A(4)=-0.4082 A(7)=0.2342 A(2)=0.8699 A(5)=0.6216 A(8)=-0.0915 A(3)=-0.0401 A(6)=0.2569 A(9)=0.9458	ResNorm(1)=0.0870 ResNorm(2)=2.0753 ResNorm(3)=0.3441
9	X=-0.2240 Y=0.1797 Z=0.3102	0.1355	X=2.5615 Y=4.0430 Z=1.1660	A(1)=-0.0728 A(4)=-0.9745 A(7)=-0.1602 A(2)=1.1269 A(5)=0.3880 A(8)=-0.2173 A(3)=0.0426 A(6)=0.1223 A(9)=0.8202	ResNorm(1)=0.1249 ResNorm(2)=1.5417 ResNorm(3)=0.8120
10	X=0.0787 Y=0.1014 Z=-0.0933	0.0649	X=3.5825 Y=4.4535 Z=3.7836	A(1)=0.0252 A(4)=-0.9551 A(7)=0.1843 A(2)=0.9507 A(5)=0.0518 A(8)=-0.4058 A(3)=-0.0026 A(6)=-0.0006 A(9)=0.9899	ResNorm(1)=0.0082 ResNorm(2)=0.0006 ResNorm(3)=0.5599
11	X=0.0662 Y=-0.2012 Z=-0.4430	0.0834	X=3.7216 Y=4.4707 Z=4.3570	A(1)=0.0519 A(4)=-0.9726 A(7)=0.1543 A(2)=0.9078 A(5)=-0.0946 A(8)=-0.4708 A(3)=-0.0017 A(6)=0.0283 A(9)=1.0464	ResNorm(1)=0.0302 ResNorm(2)=0.0711 ResNorm(3)=0.8382
AVERAGE	N/A	0.1984	X=3.6297 Y=3.9050 Z=2.8050	N/A	N/A
Comments	We have detailed one deformation for each	Similar value compared to 1Voxel 2D	In Simulation 8 there	The optimization Process was carried out with Matlab row by row independently. That	The Optimization is made row by row. We have three rows in

	coordinate, but there are sometimes additional deformation in 1-4 more coordinates.	Simulations. *See Error Calculations Formulas.	is an important difference in z coordinate, which makes the average value biased.	explains why we have got 3 Residual Norms values.	the matrix of Equation 81. Therefore, there are three ResNorm values. ResNorm is the residual after the Optimization.

Table 4.-The results for 11 random simulations in 3D for 1 voxel. The average RMS error is about 20%.

3D SIMULATIONS FOR 2 VOXELS					
Simulation	Random Value of Deformation(s) (Approximated) and Coordinate(s) where they are applied on	RMS Error (Average for X,Y and Z Coordinates*)	IRC Approximated for 2 Voxels	Optimized Rotation Matrix (Pseudo-Orthogonal)	Optimization Residuals
1	Y=0.5 , -0.5 0.5 , -0.5	0.0892	X=3.7500 Y=4.3667 Z=4.1167	A(1)=0.1331 A(4)=-0.9845 A(7)=0.2705 A(2)=0.8691 A(5)=-0.0096 A(8)=-0.2658 A(3)=0.0322 A(6)=-0.0250 A(9)=0.9646	ResNorm(1)=0.7085 ResNorm(2)=0.9913 ResNorm(3)=0.8755
2	Y=-1 , -0.2 -0.2 , -0.2	0.0973	X=3.2429 Y=4.5924 Z=2.8399	A(1)=-0.0054 A(4)=-1.1257 A(7)=0.3639 A(2)=1.2301 A(5)=-0.2349 A(8)=-0.3527 A(3)=0.0372 A(6)=0.0634 A(9)=0.9931	ResNorm(1)=1.7523 ResNorm(2)=0.8797 ResNorm(3)=0.4367
3	Y=0.25 , -0.25 0.25 , -0.25	0.0621	X=3.6250 Y=4.4524	A(1)=0.0617 A(4)=-0.9865 A(7)=0.2930 A(2)=0.9378 A(5)=-0.0103 A(8)=-0.2872	ResNorm(1)=0.1505 ResNorm(2)=0.2711

			Z=3.8274	A(3)=0.0088 A(6)=-0.0109 A(9)=0.9772	ResNorm(3)=0.7238
4	Y=0.75 , -1 0.75 , -1	0.1316	X=3.8516 Y=4.2188 Z=4.2734	A(1)=0.2245 A(4)=-1.0476 A(7)=0.2347 A(2)=0.8096 A(5)=-0.0479 A(8)=-0.2545 A(3)=0.0823 A(6)=-0.0432 A(9)=0.9402	ResNorm(1)=1.8483 ResNorm(2)=2.6963 ResNorm(3)=1.0630
5	Y=0.35 , 0.35 -0.75 , -0.75	0.0869	X=3.6700 Y=4.4197 Z=3.9297	A(1)=0.0906 A(4)=-1.0392 A(7)=0.2821 A(2)=0.9124 A(5)=-0.0905 A(8)=-0.2805 A(3)=0.0171 A(6)=-0.0146 A(9)=0.9716	ResNorm(1)=0.3206 ResNorm(2)=1.3471 ResNorm(3)=0.7781
6	X=0.4134 Y=0.1324 Z=-0.4025	0.1934	X=7.6358 Y=4.6284 Z=8.8630	A(1)=0.6503 A(4)=-0.3884 A(7)=0.5600 A(2)=0.8495 A(5)=-0.3681 A(8)=-0.7985 A(3)=0.0468 A(6)=0.0950 A(9)=0.5469	ResNorm(1)=5.3957 ResNorm(2)=4.1993 ResNorm(3)=1.5121
7	X=0.5202 Y=0.2746	0.0616	X=3.5000 Y=4.3200 Z=3.3200	A(1)=0.0516 A(4)=-0.9936 A(7)=0.3030 A(2)=0.9298 A(5)=0.1444 A(8)=-0.2770 A(3)=0.0017 A(6)=0.0221 A(9)=0.9843	ResNorm(1)=0.1116 ResNorm(2)=0.3168 ResNorm(3)=0.7078
8	X=0.4966 Y=0.5283 Z=0.2760	0.1096	X=4.9076 Y=6.9978 Z=10.2205	A(1)=-0.2764 A(4)=-0.1817 A(7)=0.2264 A(2)=1.0263 A(5)=0.1785 A(8)=0.0549 A(3)=-0.0507 A(6)=0.1973 A(9)=1.0269	ResNorm(1)=0.4021 ResNorm(2)=2.8940 ResNorm(3)=0.2720
9	X=-0.2240 Y=0.1797	0.1581	X=-3.7884 Y=7.0361	A(1)=0.7478 A(4)=-0.8034 A(7)=0.0088 A(2)=0.7073 A(5)=0.3705 A(8)=-0.2146	ResNorm(1)=4.0591 ResNorm(2)=2.8513

	Z=0.3102		Z=-16.2613	A(3)=0.2451 A(6)=0.1839 A(9)=0.9355	ResNorm(3)=0.5123
10	X=0.0787 Y=0.1014 Z=-0.0933	0.0241	X=3.5000 Y=4.5570 Z=3.5570	A(1)= -0.0269 A(4)=-0.0910 A(7)=0.3264 A(2)=0.09943 A(5)=0.0515 A(8)=-0.3295 A(3)=-0.0036 A(6)=0.0009 A(9)=1.0127	ResNorm(1)=0.1143 ResNorm(2)=0.0750 ResNorm(3)=1.0067
11	X=0.0662 Y=-0.2011 Z=-0.4430	0.0994	X=3.5000 Y=4.7978 Z=3.7978	A(1)=-0.2053 A(4)=-0.7983 A(7)=0.4157 A(2)=0.8607 A(5)=0.1255 A(8)=-0.2476 A(3)=-0.0143 A(6)=0.0291 A(9)=1.0398	ResNorm(1)=1.5171 ResNorm(2)=1.7608 ResNorm(3)=2.0541
AVERAGE	N/A	0.1010	X=4.0883 Y=4.9443 Z=2.9531	N/A	N/A
Comments		It is clearly about 10% less than 1Voxel 3D Simulations, and even lower than 2 Voxels 2D Simulations. But we consider that.	Large deviations in some values.		

Table 5.-Here we show the results for 11 **3D** simulations with 2 voxels. We find out acceptable Error values of about 10% on average. Statistically speaking, about 25 Simulations samples would be more contundent to set the proof.

```
% Random Values Deformations a=(rand(1)-0.5)
b=(rand(1)-0.5)
% Points of Voxel(s) x1=2;
y1=7; x2=1; y2=6; x11=6; y11=6+a x22=5; y22=7+b
% straight lines (Reuleaux
% Segments) Equations m1=(y11-y1)/(x11-x1);
m2=(y22-y2)/(x22-x2); m11=-1/m1;
m22=-1/m2;
% middle points mpx1=(x1+x11)/2; mpy1=(y1+y11)/2; mpx2=(x2+x22)/2;
mpy2=(y2+y22)/2; b1=mpy1-m11*mpx1; b2=mpy2-m22*mpx2;
% Reuleaux point b=[-b1
  -b2]; m=[m11 -1
  m22 -1];
r=inv(m)*b xr=r(1,1)
yr=r(2,1)
% translated points to the
% Coordinates Center (initial
% position ti, final position tf) xti=[x1-xr
   y1-yr x2-xr y2-yr]
xtf=[x11-xr
   y11-yr x22-xr y22-yr]
```

Fig 10.-On the left, we show an example of the simplest Matlab program for the determination of the IRC through the **NRM** in **2D**. We have taken only two Reuleaux Segments. Usually, when working with 1 voxel, we take 4 Reuleaux Segments, 2 on the top-border points of the **PRB**, and other 2 on the inferior-border part of **the PRB**, and calculate the average value for the 2 IRCs obtained. The reader can edit more improved and refined programs with this frame, both in **2D** and **3D**.

Cite this Article

Francisco Casesnoves , "Software-Engineering Optimization with Mathematical Method Improvements for Numerical Reuleaux Method", International Journal of Scientific Research in Science, Engineering and Technology (IJSRSET), Online ISSN : 2394-4099, Print ISSN : 2395-1990, Volume 7 Issue 2, pp. 447-499, March-April 2020. Available at doi : https://doi.org/10.32628/IJSRSET19648
Journal URL : http://ijsrset.com/IJSRSET19648